POLARIZATION EFFECTS OF NONSPHERICAL SCATTERERS IN DIELECTRIC OPTICAL FILM

A Thesis Submitted to
the Graduate School of Engineering and Sciences of
İzmir Institute of Technology
in Partial Fulfillment of the Requirements for the Degree of

MASTER OF SCIENCE

in Electronics and Communication Engineering

by
Nasrettin YUNUS

July 2007
İZMİR

We approve the thesis of **Nasrettin YUNUS**

Date of Signature

. . . . . **20 July 2007**
Assoc. Prof. Dr. M. Salih DİNLEYİCİ
Supervisor
Department of Electrical and Electronics Engineering
İzmir Institute of Technology

. . . . . **20 July 2007**
Assist. Prof. Dr. Şevket GÜMÜŞTEKİN
Department of Electrical and Electronics Engineering
İzmir Institute of Technology

. . . . . **20 July 2007**
Assist. Prof. Dr. Yeşim Zoral YÜKSEL
Department of Electrical and Electronics Engineering
Dokuz Eylül University

. . . . . **20 July 2007**
Prof. Dr. F.Acar SAVACI
Head of Department
İzmir Institute of Technology

. . . . . .
Prof. Dr. M. Barış ÖZERDEM
Head of the Graduate School

ACKNOWLEDGEMENTS

I would like to give special thanks to my supervisor Associate Prof.Dr.Salih Dinleyici. His guidance, encouragement and support definitely had a substantial impact on my approach to a problem. He has been a kind advisor, teacher and friend.

I want to thank Assist. Prof.Dr.Şevket Gümüştekin, for his support and useful discussions. I greatly appreciate his time and effort for various parts of this work.

I like to thank Prof.Dr.Ferit Acar Savacı, for his motivations and guidence during lecture times.

I would also like to thank my friend Osman Akın for his accompanying me several times in experimental studies.

I am so grateful to my wife, Ceylan, for her help, love and support. She has always been supportive of my work and encouraged me to achieve my career goals. And finally, I want to thank my sun, Ali Emre, because of his patience, love and moral support those have always given me energy to work.

ABSTRACT

POLARIZATION EFFECTS OF NONSPHERICAL SCATTERERS IN DIELECTRIC OPTICAL FILM

Polarization enhancement in liquid crystal display (LCD) backlighting systems comprises important part of works on improvement of the brightness. Optical films containing scatterer particles are used in these systems. Therefore, dielectric scatterer particles are greatly needed to be analyzed for their optical scattering properties, and especially for polarizing effects.

Depending on the sizes relative to the wavelength and the shape of the particles various computation approaches have been developed based on electromagnetic scattering theories such as Mie scattering, T-matrix methods etc... Simulation programs of these approaches have been examined and applied for spherical and nonspherical particles. In general, for the particles those a few times large in size compared to the incident wavelength, the polarization differentiation is insignificant for a spherical particle compared to a spheroid one. And, the prolate spheroids with higher aspect ratio have been able to produce most significant differentiating figures.

Polarization measurements have been carried on commercially available dielectric optical films of two different set and also on the films with/without nonspherical zeolite particles prepared in the laboratory. Since the commercial films consist of spherical scatters, they show no polarization discrimination at all. On the other hand existence of zeolite particles in the film resulted in significant polarization discrimination at forward scattering angle.

The results for polarization discrimination properties of the prolate spheroid particles have been compared with the spherical ones. Consequently, the discrepancy induced on the polarization that way has a good potential to be used in improvement of the brightness.

ÖZET

DİELEKTRİK OPTİK FİLM İÇERİSİNDEKİ KÜRESEL OLMAYAN SAÇICILARIN POLARİZASYON ETKİLERİ

Likit kristal ekran (LCD) gibi birçok görüntüleme sisteminde kullanılan arkaışık ünitelerinde polarizasyonu arttırma çalışmaları, parlaklık seviyesini iyileştirme çabaları içinde çok önemli bir yer tutmaktadır. Bu nedenle, içerisinde veya üzerinde saçıcı partiküllerin bulunduğu optik filmlerin polarizasyona etkisinin çok iyi incelenmesi gerekmektedir.

Farklı biçim ve boyutlara (dalgaboyuna göre) sahip partiküllerin saçılma hesaplamaları için elektromanyetik kuramı esaslı çok iyi bilinen (Mie kuramı, T-Matris) birçok yaklaşım geliştirilmiştir. Bu yaklaşımları kullanan benzetim programları incelendi, en uygun biçim ve boyutun bulunması için kullanıldı. Dalgaboyunun bir kaç katı büyüklükte olan partiküller ileri yönde saçılma yaparken dar bir saçılma açısı içerisinde polarizasyon ayrışması yapabilmektedir. Bu uygulama açısından gerek duyulan bir durumdur. Genel olarak küresel saçıcılar simetri nedeniyle polarizasyon ayrışması yapamaz, ancak küresel olmayan, küremsi partiküller bunun tam tersi bir özellik gösterebilmektedir. Yayvan küremsi partiküller yüksek boyut oransalıyla en fazla polarizasyon ayrışması göstermektedir.

Polarizasyon karakterizasyon ölçümleri, standart olarak bulunan iki farklı sete ait optik filmler için gerçekleştirilmiştir. Küresel saçıcıların bulunduğu bu filmlerde hiçbir polarizasyon ayrışması gözlenmedi. Ayrıca içerisinde zeolite (küresel olmayan saçıcı) bulunan ve bulunmayan optik filmler üzerinde yapılan ölçümler, ileri yönde saçılmalarda önemli bir polarizasyon farklılaşması olduğunu göstermiştir.

Dielektrik yayvan küremsi saçıcıların polarizasyon ayrıştırma özelliği küresel saçıcılarınki ile karşılaştırıldı. Polarizasyonda oluşan bu farklılaşma parlaklık değerini artırmak amacıyla kullanılma potansiyeline sahiptir.

TABLE OF CONTENTS

LIST OF FIGURES

Figure **Page**

LIST OF TABLES

CHAPTER 1

INTRODUCTION

Various organic and inorganic materials that showing very diverse optical properties have been studied and used in industries related to electronics, optics and photonics. Optical thin films as a specialized area find many application opportunities in display technologies due to their optical properties those can be altered via infinite chemical compositions and morphological structures. Changes induced by optical thin films on the polarization properties of an incident light wave depend on morphological asymmetry in the structure of the film. This anisotropic structure can change the orientation and the polarization state of passing light waves according to purpose. There exist many aspects in investigations of light-scattering and polarization properties of surfaces and thin films. Mathematical modeling of single scatter and polarization properties of the film obtained by these scatters are computational side of the research interest. On the other hand production of those polymeric films with suitable scatter geometry is another side but not considered in this thesis. Only a few polymeric films developed in Chemical Engineering Department with zeolites and commercially available ones are tested for polarization characterization.

Diffuser polymeric films and plates used in most liquid crystal display (LCD) backlighting systems have been employed for controlling the unpolarized or partially polarized light generated by CCFLs (Cold Cathode Fluorescent Lamb) in order to obtain a uniform light intensity (brightness) distribution. This intensity distribution should also be uniform in spectral domain for visible range. Moreover, the intensity distribution should be within an angle defined by the viewer which is called viewing angle. Favored polarization state might be desired in some cases for further increase in brightness by recycling orthogonal polarization state instead of wasting this as in usual classical systems. In general the films are made of polymeric substrate with various scatters which may vary in size, shape and optical properties, namely refractive indices. Typically, the diffusing films contain spherical scatters either on the surface or in the substrate that show no polarization effect due to symmetric structure. In this study, polymeric diffusing films having dielectric nonspherical (spheroid) scatters which are expected to show high polarizing discrimination property. Especially those films having

scatters 4-5 times large in size compared to the wavelength will be investigated for brightness enhancement purposes, at the same time keeping the uniformity at the acceptable level. The sizes of the scatters are dictated and required by forward scattering needs such as that the most of the light should be within forward direction. Light scattered by the substrates consisting of dielectric particles with sizes significantly larger than the wavelength exhibit also a polarization discrimination at small scattering angles (Yevgen et al. 2006) which is very suitable with the requirement of diffusing optical films in display technology applications.

Theoretical background for polarization optics is given in Chapter 2. Polarized or partially polarized light can be represented by vectors (Jones and Stokes vectors) and propagation of these vectors for the given medium is characterized by 2x2 or 4x4 matrices. When polarized light is incident on a sample at an oblique angle of incidence, the light scattered by this sample has a polarization that dependent upon the optical properties of scattering sources and observation angle. Electromagnetic theory aspects of polarization and polarizing devices with special properties are also placed in this chapter.

In Chapter 3, the polarization properties of the scatters are investigated. General scattering analysis of spherical scatters is introduced and mathematical model of Mie scattering based on stokes vector representation is explained. Mie theory is a complete mathematical-physical theory of the scattering of electromagnetic wave by homogeneous spherical particles in a non-absorbing medium. The computational approach exploited in a number of simulation programs is detailed and some results of which will be used for comparison with nonspherical particle case are presented in intensity and scattering angle graphics.

Chapter 4 concentrates on nonspherical geometries of particles, such as spheroids and ellipsoids. Scattering by dielectric particles displays a significant dependence on shape of particle. Although Mie theory embraces all possible ratios of the particle radius to wavelength of incidence light, the theory is restricted to spherical particles and it is not convenient to use in nonspherical particles used in this study. More advanced scattering theories have been developed after Mie theory for the analyzing scattering properties of nonspherical particles. A number of methods developed for arbitrarily shaped particles can be classified into two groups: Volume base methods generally used for the inhomogeneous particles and surface base methods those sufficient to analyze scattering from homogeneous ones. The execution time of

the scattering codes based on volume base methods is rather long since the whole volume of a particle is needed to be analyzed. In this study, Chapter 4 describes a surface base technique called T-matrix method, for computing electromagnetic scattering by single, homogenous, and arbitrarily shaped particles. It is considered of advantage to perform scattering computations since all information on the polarization scattering effects is included in the T-matrix. The simulation results obtained from scattering software based on T-matrix method are also included in this chapter.

In chapter 5, polarization properties of commercially available optical films for two different sets of backlight units are experimentally investigated. Also, polarization properties of a dielectric optical film deposited with zeolites particles are measured in our optical laboratory. Measurements for polarization properties of light and characterization of the medium can generally be done by an ellipsometer. Since, our experimental works require measurements in small angle of deviation (scattering angle) a simple set-up at two wavelengths (632.5 nm and 542 nm) is used with necessary optical detectors and components to measure polarization coefficient as explained in the chapter.

Chapter 6 completes with a discussion on how a spheroid particle can help to improve brightness of the display system in comparison with a spherical particle. Polarization characteristics of optical films containing zeolite particles are also discussed and commented for feedback on further studies in production method.

CHAPTER 2

POLARIZATION OF LIGHT

2.1. Introduction

Polarization is one property of light waves which can be described by classical electromagnetic theory. Light have both particle-like and wave-like properties. Polarization deals with the wave-like properties of light.

Electromagnetic waves have both electric and magnetic fields denoted as $\boldsymbol{E}$ and $\boldsymbol{H}$, respectively. Both are functions of time and space. They are complex and have real and imaginary parts.

The flow of Electromagnetic energy is given by the Poynting vector $\boldsymbol{S}$:

$$\boldsymbol{S} = \frac{c}{4\pi}(\boldsymbol{E} \times \boldsymbol{H}) \tag{2.1}$$

The direction of energy flow (polarization) is determined by the $\boldsymbol{S}$ vector. The direction of $\boldsymbol{S}$ vector is orthogonal to both $\boldsymbol{E}$ and $\boldsymbol{H}$ according to the (2.1). Polarization effects are related to the $\boldsymbol{E}$ vector. That is, the plane of polarization is defined as the plane in which the $\boldsymbol{E}$ vector is oscillating.

2.2. State of Polarization

Each vibrating atom or molecule emits linearly polarized light. But the individual atoms or molecules generally may not act together, so their vibrations have no fixed phase relationships and cannot be added into a single linearly polarized beam. Thus, we must call light from natural sources such as the sun, a candle flame, or an electric light bulb unpolarized.

In an unpolarized light beam, the $\boldsymbol{E}$ vector vibrates in all directions perpendicular to the direction of propagation. If a snapshot is taken at a particular instant of time, different parts of the beam will have $\boldsymbol{E}$ vectors vibrating with different

amplitudes and phases at different angles to each other, but all in a plane perpendicular to the direction of propagation as shown in Fig.2.1.

Figure 2.1. Unpolarized light

Real part of a homogeneous harmonic plane wave can be defined as shown in Equation (2.2) where ***r****(x, y, z)* is a position vector of a point in space and ***k****(k_x, k_y, k_z)* a unit vector in a fixed position.

$$\boldsymbol{E}(r,t) = E_0 cos\left[2\pi v\left(t - \frac{\boldsymbol{r.k}}{c} \right) + \varphi \right] \tag{2.2}$$

Waves can be combined by conventional vector addition methods. So the ***E*** vector can be separated into two components (Such as $\boldsymbol{E_x}$ and $\boldsymbol{E_y}$) in mutually perpendicular directions that are vibrating in phase. For a monochromatic plane wave traveling in the *z* direction with frequency v and velocity *c*, the *x* and *y* components of the wave are,

$$\boldsymbol{E}_x = E_{0x} cos\left[2\pi v\left(t - \frac{z}{c} \right) + \varphi_x \right] \tag{2.3a}$$

$$\boldsymbol{E}_y = E_{0y} cos\left[2\pi v\left(t - \frac{z}{c} \right) + \varphi_y \right] \tag{2.3b}$$

$$\boldsymbol{E}(z,t) = \boldsymbol{E}_x \hat{x} + \boldsymbol{E}_y \hat{y} \tag{2.3c}$$

where φ_x and φ_y are the phases respectively. Using conventional vector addition methods, the resultant electric field vector ***E*** will trace out an ellipse (see Fig. 2.2) that is perpendicular to the wave vector k,

$$\left(\frac{\boldsymbol{E}_x}{E_{0x}}\right)^2+\left(\frac{\boldsymbol{E}_y}{E_{0y}}\right)^2-2\left(\frac{\boldsymbol{E}_x}{E_{0x}}\right)\left(\frac{\boldsymbol{E}_y}{E_{0y}}\right)cos\varphi=sin^2\varphi \tag{2.4}$$

where the phase difference $\varphi=\varphi_y-\varphi_x$. The intensity I is determines by the size of the ellipse as the equation below where η is the impedance of the medium.

$$I=(E_{0x}^2+E_{0y}^2)/2\eta \tag{2.5}$$

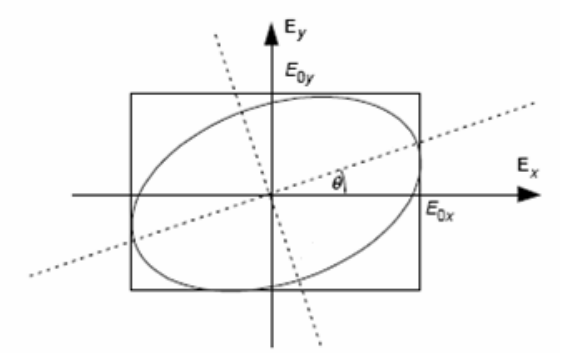

Figure 2.2. Polarization ellipse

The state of polarization is, related to shape of the ellipse (Saleh 1991) determined by the ratio E_{0y}/E_{0x} and the phase difference φ. Generally, at a particular time t, $\boldsymbol{E}$ follows a trajectory according to Equation (2.4) lying on the surface of an elliptical cylinder.

A particular light wave can be referred in terms of its specific state of polarization. Linearly polarized or plane-polarized light is said to be in a *P*-state and right- or left-circular polarized light is referred as *R*- and *L*-state, respectively. The condition of elliptical polarization corresponds to an *E*-state.

2.2.1. Linearly Polarized Light

For linearly polarized light, if a snapshot of a light beam is taken at a particular instant, the $\boldsymbol{E}$ vector will be vibrating at a certain angle in the *x*–*y* plane. As time or position varies, the amplitude of the $\boldsymbol{E}$ vector will vary in a sinusoidal manner, but the vibration will remain at the same angle in the *x*–*y* plane. Whit this point of view if one of the components vanishes, the light is linearly polarized in the direction of the other

component. The wave is again linearly polarized if the phase difference $\varphi = m\pi$ for ($m=0, \pm 1, \pm 2\ldots$) since (2.3) gives

$$\boldsymbol{E}_y = \pm \frac{E_{0y}}{E_{0x}} \boldsymbol{E}_x \tag{2.6}$$

which is the equation of a straight line (the + sign correspond to $\varphi = 0$ and – sign to $\varphi = (2m+1)\pi$). For $E_{0y} = 0$ or $E_{0x} = 0$ the plane of polarization is the *x*-*z* plane and *y*-*z* plane respectively. If $\varphi = (2m+1)\pi$ and $E_{0y} = E_{0x}$, the plane of polarization will have an angle 45^0 with the *x* axis. Fig. 2.3 shows the wave representations of the linearly polarized light where $E_{0y} = 0$.

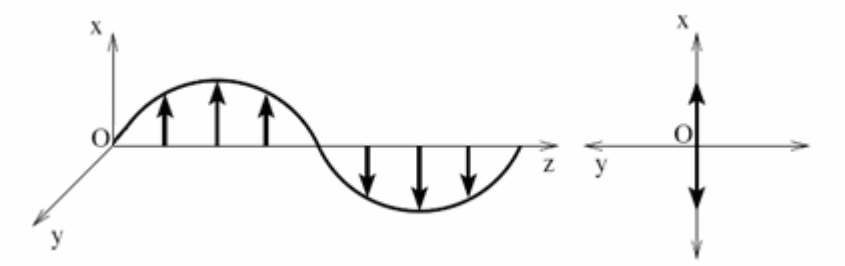

Figure 2.3. An illustration of a linearly polarized light wave where $E_{0y} = 0$

2.2.2. Circularly Polarized Light

For circularly polarized light, if a snapshot of a light beam is taken at a particular instant, the ***E*** vector sweeps out a circle in the *x*–*y* plane. In this case phase difference $\varphi = \pm \pi/2$ and the two components $\boldsymbol{E_x}$ and $\boldsymbol{E_y}$ have the same amplitude $E_{0y} = E_{0x} = E_0$, so (2.3) gives

$$\boldsymbol{E}_x = E_0 cos\left[2\pi v\left(t - \frac{z}{c} \right) + \varphi_x \right] \tag{2.7a}$$

$$\boldsymbol{E}_y = \pm E_0 sin\left[2\pi v\left(t - \frac{z}{c} \right) + \varphi_y \right] \tag{2.7b}$$

from the circle equation that $\boldsymbol{E}_x^2 + \boldsymbol{E}_y^2 = E_0^2$. In circular polarization state the elliptical cylinder in Fig. 2.1 becomes a circular shape as illustrated in Fig. 2.4.

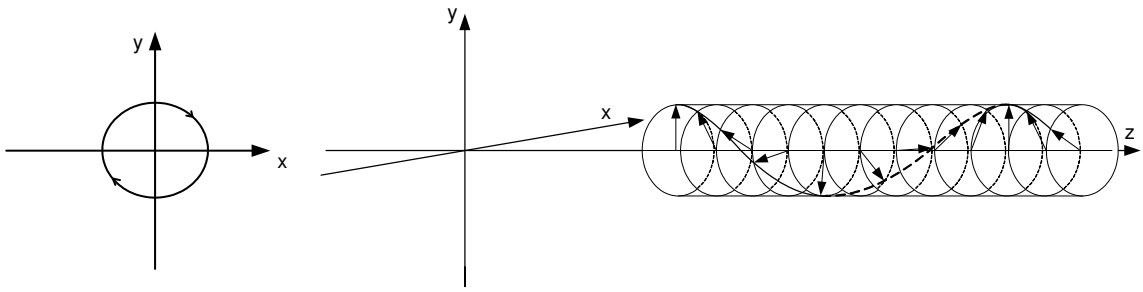

Figure 2.4. Circular polarization

In the case $\varphi = +\pi/2$ the electric field at a particular position z vibrate in a clockwise direction when viewed from the direction toward which the wave is approaching. Then the light is said to be right circularly polarized. The other case $\varphi = -\pi/2$ corresponds to left circularly state with counterclockwise rotation.

2.3. Matrix Representations of Polarization

In order to characterize the propagation of light and the effect of optical devices, several matrix methods have been developed (Born and Wolf 1986). In optical systems, generally there exist an incident beam (in matrix form) and a device (also in matrix form) that alters the state of polarization of the incident beam. The exiting beam will be in another state of polarization and also expressed with a third matrix, as product of the first and second matrices. The most common matrix representation methods are the Jones calculus and the Mueller calculus.

There is also a visual method called Poincare´ sphere on which vectors represent different states of polarization.

2.3.1. The Jones Vector

The Jones vector, developed by Clark Jones in 1941, is a two-component column vector that contains information about the amplitude properties of the beam.

The Jones calculus is more convenient to handling the phases of light wave problems. The Jones vector cannot be used to handle polarization problems (Guenther, 2005).

The general form of the Jones vector is:

$$J = \begin{pmatrix} A \\ B \end{pmatrix} \tag{2.8}$$

The normalized vector is the terms contained within the bracket, each divided by $1/\sqrt{2}$.

A monochromatic plane wave describing in (2.3) is can be completely characterized by the complex envelopes A_x and A_y:

$$A_x = E_{0x} exp(j\varphi_x) \tag{2.9a}$$

$$A_y = E_{0y} exp(j\varphi_y) \tag{2.9b}$$

It is convenient to write this complex representation with respect to Jones vector as

$$J = \begin{pmatrix} A_x \\ A_y \end{pmatrix} \tag{2.10}$$

According to (2.10), the total intensity I and the state of polarization ellipse can be determined by using (2.11) and (2.12) respectively.

$$I = \frac{\left(|A_x|^2 + |A_y|^2\right)}{2\eta} \tag{2.11}$$

$$\frac{E_{0y}}{E_{0x}} = \frac{|A_y|}{|A_x|} \quad and \quad \varphi = \varphi_y - \varphi_x = arg\{A_y\} - arg\{A_x\} \tag{2.12}$$

Some examples of Jones vectors representing some special polarization states are shown in Table 2.1.

Table 2.1. Jones vectors for different states of polarizations

Linearly polarized wave making angle θ with x axis	$\begin{pmatrix} cos\theta \\ sin\theta \end{pmatrix}$	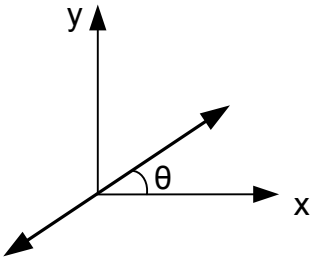
Linearly polarized wave, in x direction	$\begin{pmatrix} 1 \\ 0 \end{pmatrix}$	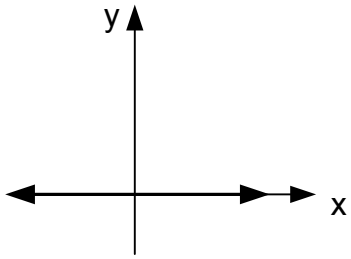
Right circularly polarized wave	$\frac{1}{\sqrt{2}}\begin{pmatrix} 1 \\ j \end{pmatrix}$	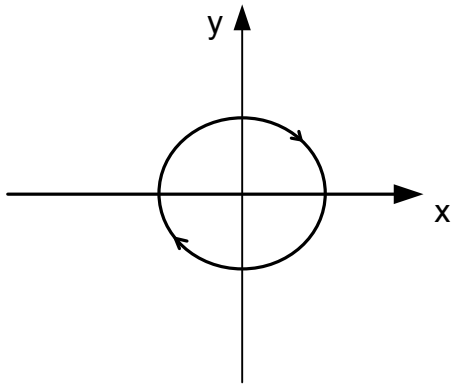
Left circularly polarized wave	$\frac{1}{\sqrt{2}}\begin{pmatrix} 1 \\ -j \end{pmatrix}$	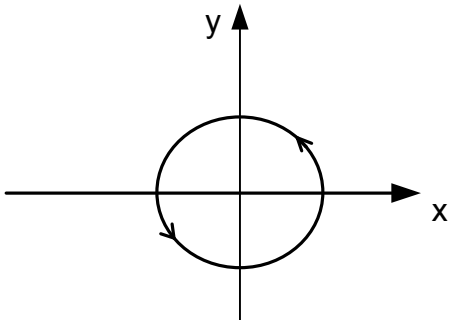

2.3.2. Stokes Vector and Mueller Matrix Representation

Stokes vector is a *4 x 1* vector, determined by a set of six intensity measurements recorded through a set of various polarizing filters. It is a representation of the polarization state of light. It can be shown as below column matrix:

$$S = \begin{pmatrix} I \\ Q \\ U \\ V \end{pmatrix} = \begin{pmatrix} I_X + I_Y \\ I_X - I_Y \\ I_P - I_M \\ I_R - I_L \end{pmatrix} \tag{2.13}$$

where the subscripts *X, Y, P, M, R*, and *L* stand for horizontal linear, vertical linear, $+45^o$ linear, -45^o linear, right circular, and left circular states of polarization, respectively. *I* is the intensity after the respective polarizing filters. $I_x = E_x E_x^*$ and $I_y = E_y E_y^*$ are used instead of *I* and *Q* in an alternative system.

The Stokes parameters can be used in both monochromatic and quasi-monochromatic waves for characterization of the state of polarization. The vector can represent not only polarized 1ight, but also unpolarized or partially polarized light.

The general Stokes parameters of any light wave may be determined from simple experiments as below:

$$\left.\begin{aligned} I &= \left\langle E_{0x}^2 \right\rangle + \left\langle E_{0y}^2 \right\rangle, \\ Q &= \left\langle E_{0x}^2 \right\rangle - \left\langle E_{0y}^2 \right\rangle, \\ U &= 2\left\langle E_{0x} E_{0y} cos\varphi \right\rangle, \\ V &= 2\left\langle E_{0x} E_{0y} sin\varphi \right\rangle, \end{aligned}\right\} \tag{2.14}$$

where time average is denoted by $\langle . \rangle$. The first element, *I*, represents the total intensity of light. The second element, *Q*, indicates the tendency of light; if $Q>0$ to horizontal polarization, and if $Q< 0$ to vertical polarization. Similarly, *U* shows the tendency of the

light to be $\pm 45^0$ linearly polarized and V indicates the tendency to R or L circularly polarization (Born and Wolf 1999).

The interaction of light with optical elements such as lens system, polarizers, filters, scattering media etc, changes the polarization state of the light. Typical Stokes vectors are shown in Table 2.2.

Table 2.2. Typical Stokes Vectors

Linearly polarized wave making angle $\theta=45^0$ with x axis	$\begin{pmatrix} 1 \\ 0 \\ 1 \\ 0 \end{pmatrix}$	Linearly polarized wave making angle $\theta=-45^0$ with x axis	$\begin{pmatrix} 1 \\ 0 \\ -1 \\ 0 \end{pmatrix}$
Linearly polarized wave, in x direction	$\begin{pmatrix} 1 \\ 1 \\ 0 \\ 0 \end{pmatrix}$	Linearly polarized wave, in y direction	$\begin{pmatrix} 1 \\ -1 \\ 0 \\ 0 \end{pmatrix}$
Right circularly polarized wave	$\begin{pmatrix} 1 \\ 0 \\ 0 \\ 1 \end{pmatrix}$	Left circularly polarized wave	$\begin{pmatrix} 1 \\ 0 \\ 0 \\ -1 \end{pmatrix}$

Stokes vector provides a computational technique in the form of the Mueller matrix methods. Mueller matrix is a transformation matrix which has a capability to determine of how an optical sample interacts or transforms the polarization state of an incident light beam. This matrix operates directly on an input or incident Stokes vector, thus resulting in an output Stokes vector that define the polarization state of the emerging beam. This operation can be described by the following equation:

$$S_{out} = \boldsymbol{M}\, S_{in} \tag{2.15}$$

where, S_{out} and S_{in} are the output and incident Stokes vectors, respectively. $\boldsymbol{M}$ is the Mueller matrix of the media or optical system:

$$\boldsymbol{M} = \begin{pmatrix} m_{11} & m_{12} & m_{13} & m_{14} \\ m_{21} & m_{22} & m_{23} & m_{24} \\ m_{31} & m_{32} & m_{33} & m_{34} \\ m_{41} & m_{42} & m_{43} & m_{44} \end{pmatrix} \tag{2.16}$$

An optical system with a cascade of N such samples are described by the product of their respective Mueller matrices as below:

$$\boldsymbol{M}_s = M_N . M_{N-1} ... M_k .. M_1 \tag{2.17}$$

M_s and M_k are the Mueller matrices of the optical system and the kth sample of the system (Firdous et al. 2004).

By the use of the Mueller–Stokes matrix calculus, the analysis of the effect of different types of polarizers and the effect of retarders is made easier, coupled with the use of the Stokes vectors. To determine the Mueller matrices, one must measure the

Table 2.3. Typical optical polarizers and their Mueller matrices

Polarizer & Transmission axis	Mueller Matrix	Polarizer & Transmission axis	Mueller Matrix
Linear & Horizontal (x)	$\frac{1}{2}\begin{pmatrix} 1 & 1 & 0 & 0 \\ 1 & 1 & 0 & 0 \\ 0 & 0 & 0 & 0 \\ 0 & 0 & 0 & 0 \end{pmatrix}$	Linear & Vertical (y)	$\frac{1}{2}\begin{pmatrix} 1 & -1 & 0 & 0 \\ -1 & 1 & 0 & 0 \\ 0 & 0 & 0 & 0 \\ 0 & 0 & 0 & 0 \end{pmatrix}$
Linear & $+45^0$	$\frac{1}{2}\begin{pmatrix} 1 & 0 & 1 & 0 \\ 0 & 0 & 0 & 0 \\ 1 & 0 & 1 & 0 \\ 0 & 0 & 0 & 0 \end{pmatrix}$	Linear & -45^0	$\frac{1}{2}\begin{pmatrix} 1 & 0 & -1 & 0 \\ 0 & 0 & 0 & 0 \\ -1 & 0 & 1 & 0 \\ 0 & 0 & 0 & 0 \end{pmatrix}$
Circular & Right	$\frac{1}{2}\begin{pmatrix} 1 & 0 & 0 & 1 \\ 0 & 0 & 0 & 0 \\ 0 & 0 & 0 & 0 \\ 1 & 0 & 0 & 1 \end{pmatrix}$	Circular & Left	$\frac{1}{2}\begin{pmatrix} 1 & 0 & 0 & -1 \\ 0 & 0 & 0 & 0 \\ 0 & 0 & 0 & 0 \\ -1 & 0 & 0 & 1 \end{pmatrix}$

effects of a device on light with typical polarization states (Guenther 2005). Typical optical polarizers and their Mueller matrices are listed in Tables 2.3.

Stokes vectors can be also represented using a Poincare´ sphere, on which vectors represent different states of polarization, visually. The incident irradiance I is, corresponding to the radius of the Poincare´ sphere (which is usually assumed to be unity). The Stokes vectors Q, U, and V are simply the three Cartesian coordinates of a point on the Poincare´ sphere (Fig.2.5).

S_0 is related to the other three vectors by the relations (2.18) and (2.19) when the beam is completely polarized and partially polarized respectively.

$$I^2 = Q^2 + U^2 + V^2 \tag{2.18}$$

$$I^2 > Q^2 + U^2 + V^2 \tag{2.19}$$

The effects of various polarizations by samples are determined by displacements on the sphere. Each point on the sphere represents different polarization states. Different states of polarization are represented on the Poincare´ sphere as follows:

a) The equator represents various forms of linear polarization
b) The poles represent right- and left-circular polarization
c) Other points on the sphere represent elliptically polarized light.

The Poincare´ sphere is most useful for visualizing problems involving nonabsorbing materials and various polarization samples.

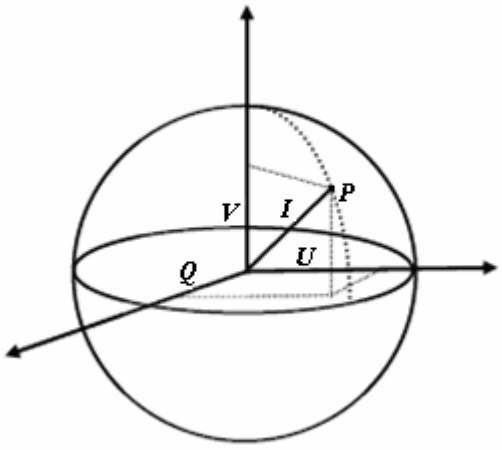

Figure 2.5. The Poincare´ sphere

2.4. Polarization Properties of Optical Filters

2.4.1. Polarizers

A polarizer is a device that generates polarized light. When the incident light is unpolarized, a linear polarizer produces light whose electric vector is vibrating primarily in one direction with only a small component vibrating in the direction perpendicular to it. Then the transmitted light is linearly polarized. A linear polarizer along *x* direction can be represented by the Jones matrix as

$$\begin{pmatrix} 1 & 0 \\ 0 & 0 \end{pmatrix}. \tag{2.20}$$

The transmittance of the light after the linear polarizer is

$$T = \frac{1}{2}(T_1 + T_2) \tag{2.21}$$

where T_1 and T_2 are the principal transmittance and the weak and perpendicular transmittance to the principal transmittance respectively.

If the incident light is linearly polarized, a linear polarizer produces a maximum value T_1 and a minimum value T_2 according to

$$T = (T_1 - T_2)\cos^2\theta + T_2 \tag{2.22}$$

where θ is the angle between the plane of polarization and the transmission axis of the polarizer. An ideal linear polarizer acts as an analyzer for the determination of the plane of polarization as shown in Fig2.6. When the incident light is linearly polarized, according to the Malus' Law, the intensity of the transmitted light from the analyzer is

$$I = I_0 \cos^2\theta \tag{2.23}$$

where I_0 is the intensity of the linearly polarized light incident to the analyzer. In the case of $\theta=\pi/2$, $I=0$ and the transmission axes of the polarizer and the analyzer are perpendicular. By rotating the analyzer and obtaining complete extinction of the light, *p*-state of light is can be detected.

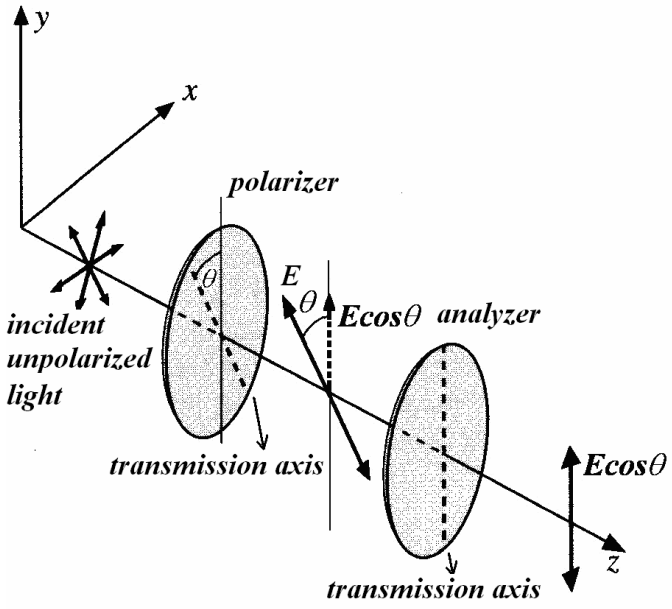

Figure 2.6. Detecting plane polarized light using polarizer as analyzer (Malus' Law)

The selective absorption of one of the two orthogonal *p*-state in incident natural light is described as dichroism. Since the dichroic polarizer is physically anisotropic, it absorbs the electric field component only in a specific direction known as the optic axis.

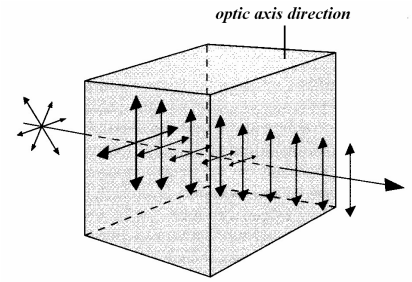

Figure 2.7. The action of a dichroic crystal as a polarizer

The electric field component perpendicular to this axis is strongly absorbed by the crystal (see Fig.2.7). The transmitted light becomes linearly polarized along the optic axis.

A Polaroid H-Sheet used in practice is a dichroic sheet polarizer. An ideal H-sheet transmits 50% of the incident natural light.

2.4.2. Retardation Plates (Retarders)

Birefringent materials show two different speeds of propagation in fixed and orthogonal directions $v_{//}$ and $v_{\perp}$ respectively. Therefore a birefringent material displays two refractive indices $n_e = c/v_{//}$ and $n_o = c/v_{\perp}$. The difference $\Delta n = n_e - n_o$ is called the birefringence. If Δn is negative the crystal is said to be uniaxial negative, conversely, if Δn is positive, the crystal is said to be uniaxial positive.

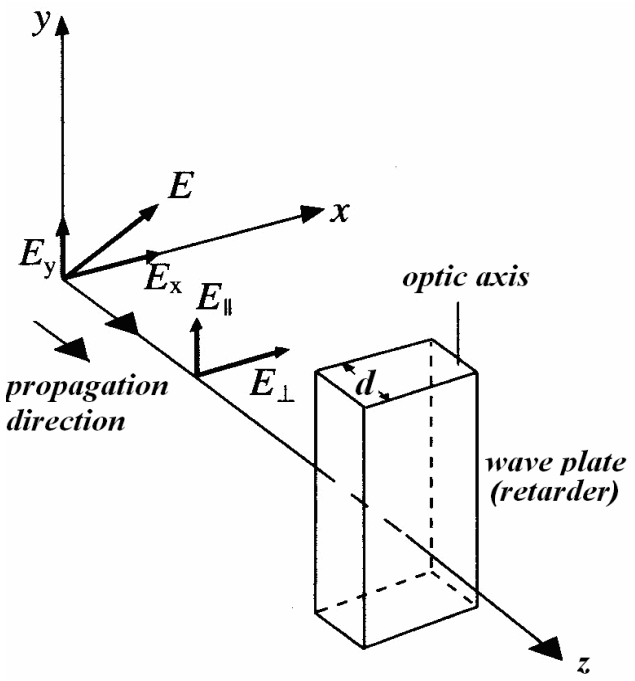

Figure 2.8. $E_{//}$ and $E_{\perp}$ propagate through the wave plate at different speeds, so that phase difference altered. The emergent light is therefore in a different state of polarization.

Retardation plates are polarization devices which delays one polarization component with respect to the other, so that they can change linearly polarized light into circularly or elliptically polarized light. They can also rotate the plane of polarization of linearly polarized light (WEB_1 2007).

In Fig2.8, components of ***E***, those extraordinary (parallel, $E_{//}=E_y$) and ordinary (perpendicular, $E_{\perp}=E_x$) to the optic axis will propagate through the retarder (a

birefringent material of thickness *d*) at different speeds and thus emerge with their phase difference alteration as

$$\Delta\varphi = (kn_e d - kn_o d) = \frac{2\pi}{\lambda}\Delta nd \tag{2.24}$$

The emergent light is therefore in a different state of polarization. Thus the Jones matrix of the retarder is

$$\begin{pmatrix} 1 & 0 \\ 0 & \exp(\Delta\varphi) \end{pmatrix} \tag{2.25}$$

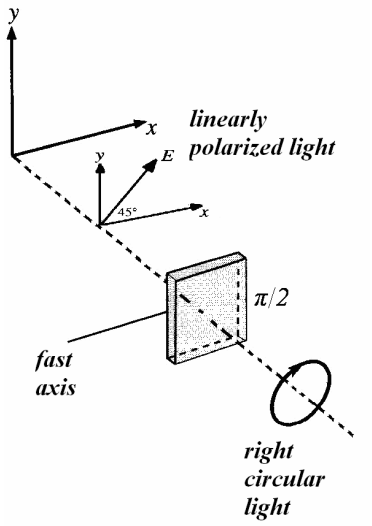

Figure 2.9. A linearly polarized wave at +45° passes through a quarter-wave plate gets converted to right circular polarization

For $\Delta\varphi=\pi/2$ (a retardation of $\lambda/4$) the retarder is a quarter-wave plate with Jones matrix

$$\begin{pmatrix} 1 & 0 \\ 0 & \exp(\pi/2) \end{pmatrix} = \begin{pmatrix} 1 & 0 \\ 0 & j \end{pmatrix}. \tag{2.26}$$

When a wave with linear polarization at ±45° passes through the retarder it gets converted to left (right) circular polarization (see Fig.2.9):

$$\left.\begin{aligned}\frac{1}{\sqrt{2}}\begin{pmatrix}1\\ j\end{pmatrix}&=\frac{1}{\sqrt{2}}\begin{pmatrix}1 & 0\\ 0 & j\end{pmatrix}\begin{pmatrix}1\\ 1\end{pmatrix}\text{ or}\\ \frac{1}{\sqrt{2}}\begin{pmatrix}1\\ -j\end{pmatrix}&=\frac{1}{\sqrt{2}}\begin{pmatrix}1 & 0\\ 0 & j\end{pmatrix}\begin{pmatrix}1\\ -1\end{pmatrix}\end{aligned}\right\} \tag{2.27}$$

For $\Delta\varphi=\pi$ (a retardation of $\lambda/2$) the retarder is a half-wave plate with Jones matrix

$$\begin{pmatrix}1 & 0\\ 0 & \exp(\pi)\end{pmatrix}=\begin{pmatrix}1 & 0\\ 0 & -1\end{pmatrix}. \tag{2.28}$$

When a wave with linear polarization at θ passes through the retarder it gets converted to linear polarization at $-\theta$:

$$\left.\begin{aligned}\begin{pmatrix}1 & 0\\ 0 & j\end{pmatrix}\begin{pmatrix}\cos\theta\\ \sin\theta\end{pmatrix}&=\begin{pmatrix}\cos\theta\\ -\sin\theta\end{pmatrix}\\ &=\begin{pmatrix}\cos(-\theta)\\ \sin(-\theta)\end{pmatrix}\end{aligned}\right\} \tag{2.29}$$

There are also variable retardation plates whose retardation can be varied in a variety of ways. Such devices are allowed a continuous adjustment of the relative phase shift, the retardance, and called compensator.

2.4.3. Polarization Rotators

A Polarization rotator rotates the plane of polarization of a linearly polarized wave by an angle θ, while its ones matrix is

$$\begin{pmatrix}\cos\theta & -\sin\theta\\ \sin\theta & \cos\theta\end{pmatrix} \tag{2.30}$$

If the incident wave is linearly polarized at angle θ_1, then the emerging light after rotator is linearly polarized at angle $\theta_2=\theta_1+\theta$.

2.5. Polarization by Reflection

The reflection of the light incident on an object's surface is the source of an image which would be created. It is important to use an effective reflection model in imaging systems in order to obtain realistic images with fine details. In this view, the laws of reflection, refraction, and Fresnel equations are needed to be analyzed in this section.

2.5.1. The Laws of Reflection and Refraction

If a plane wave of arbitrary polarization incident at a boundary between two dielectric media assumed to be linear, homogeneous and isotropic, it is split into two waves. The first wave proceeds into the second medium called transmitted or refracted wave and the other is a reflected wave propagated back into the first medium (see Fig.2.10). These two waves are assumed to be plane, through out of the section. The refractive indices of the media are n_1 and n_2. The incident, refracted, and reflected waves are propagated in the directions specified by the unit vectors k_i, k_t, and k_r respectively.

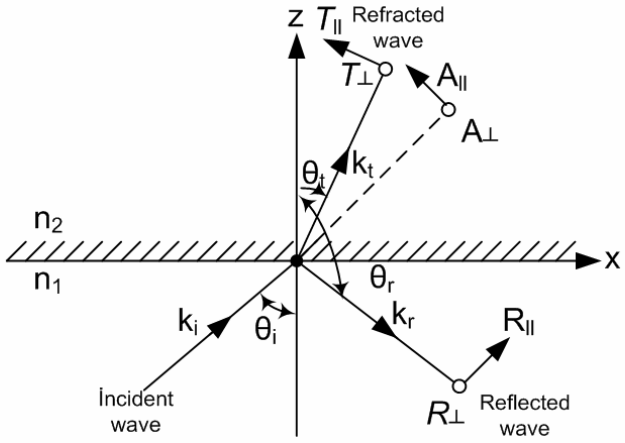

Figure 2.10. Reflection and refraction between two dielectric media

The plane specified by k_i and the normal to the boundary is called the plane of incidence. It can be shown that, according to the boundary conditions, the wavefronts of these waves are matched at the boundary if the angles of θ_i and (π-θ_r) are equal (the law of reflection) and the angles of refraction and incidence satisfies Equation 2.31:

$$n_1 \sin\theta_i = n_2 \sin\theta_t \tag{2.31}$$

The statement that the reflected wave normal k_r is in the plane of incidence, together with (2.31) is known as Snell's law or law of refraction.

2.5.2. Fresnel Formulas

If *A, T, R* are the complex amplitudes of the incident, transmitted and reflected waves, the corresponding components of the electric and magnetic vectors can be defined as shown in Table2.4 according to Fig.2.10. Each vector is resolved into components parallel (denoted by subscript ∥) and perpendicular (denoted by subscript ⊥) to the plane of incidence. The magnetic vector's components are simply obtained from (2.32) where magnetic permeability is ignored because of the media conditions. Dielectric constant is indicated as ε.

$$\boldsymbol{H} = \sqrt{\varepsilon}\boldsymbol{k} \times \boldsymbol{E} \tag{2.32}$$

The variable parts of the argument of the wave functions are taken as (2.33) where c is the velocity of propagation and ω is the angular frequency:

$$\tau_j = \omega\left(t - \frac{\boldsymbol{r}.\boldsymbol{k}_j}{c_j}\right) = \omega\left(t - \frac{x\sin\theta_j + y\sin\theta_j}{c_j}\right), \quad \text{for } j = i, r, t \tag{2.33}$$

The boundary conditions required that the tangential components of $\boldsymbol{E}$ and $\boldsymbol{H}$ should be continuous across the boundary:

$$\left.\begin{aligned} E_{ix} + E_{rx} = E_{tx}, \quad E_{iy} + E_{ry} = E_{ty}, \\ H_{ix} + H_{rx} = H_{tx}, \quad H_{iy} + H_{ry} = H_{ty}, \end{aligned}\right\} \tag{2.34}$$

Table 2.4. The components of the electric and magnetic vectors of the incident, transmitted and reflected waves

Wave	$\mathbf{E_x / H_x}$	$\mathbf{E_y / H_y}$	$\mathbf{E_z / H_z}$
Incident Wave	$E_{ix} = -A_{\|\|} \cos\theta_i e^{-j\tau_i}$ $H_{ix} = -A_{\perp}\sqrt{\varepsilon_1}\cos\theta_i e^{-j\tau_i}$	$E_{iy} = A_{\perp} e^{-j\tau_i}$ $H_{iy} = -A_{\|\|}\sqrt{\varepsilon_1} e^{-j\tau_i}$	$E_{iz} = A_{\|\|} \sin\theta_i e^{-j\tau_i}$ $H_{iz} = A_{\perp}\sqrt{\varepsilon_1}\sin\theta_i e^{-j\tau_i}$
Reflected Wave	$E_{rx} = -R_{\|\|} \cos\theta_r e^{-j\tau_r}$ $H_{rx} = -R_{\perp}\sqrt{\varepsilon_1}\cos\theta_r e^{-j\tau_r}$	$E_{ry} = R_{\perp} e^{-j\tau_r}$ $H_{ry} = -R_{\|\|}\sqrt{\varepsilon_1} e^{-j\tau_r}$	$E_{rz} = R_{\|\|} \sin\theta_r e^{-j\tau_r}$ $H_{rz} = R_{\perp}\sqrt{\varepsilon_1}\sin\theta_r e^{-j\tau_r}$
Transmitted Wave	$E_{tx} = -T_{\|\|} \cos\theta_t e^{-j\tau_t}$ $H_{tx} = -T_{\perp}\sqrt{\varepsilon_1}\cos\theta_t e^{-j\tau_t}$	$E_{ty} = T_{\perp} e^{-j\tau_t}$ $H_{ty} = -T_{\|\|}\sqrt{\varepsilon_1} e^{-j\tau_t}$	$E_{tz} = T_{\|\|} \sin\theta_t e^{-j\tau_t}$ $H_{tz} = T_{\perp}\sqrt{\varepsilon_1}\sin\theta_t e^{-j\tau_t}$

By substituting all required components from Table 2.4 into (2.34) and using the fact that $\cos\theta_r = \cos(\pi - \theta_i) = -\cos\theta_i$ and the Maxwell relation $n = \sqrt{\varepsilon}$, the Fresnel formulas are obtained in the less general form which have been first derived by Fresnel in 1823:

$$\left.\begin{aligned} T_p &= \frac{2n_1\cos\theta_i}{n_2\cos\theta_i + n_1\cos\theta_t} A_{\|\|} \\ T_s &= \frac{2n_1\cos\theta_i}{n_1\cos\theta_i + n_2\cos\theta_t} A_{\perp} \end{aligned}\right\} \tag{2.35}$$

$$\left.\begin{aligned} R_p &= \frac{n_2\cos\theta_i - n_1\cos\theta_t}{n_2\cos\theta_i + n_1\cos\theta_t} A_{\|\|} \\ R_s &= \frac{n_1\cos\theta_i - n_2\cos\theta_t}{n_1\cos\theta_i + n_2\cos\theta_t} A_{\perp} \end{aligned}\right\} \tag{2.36}$$

Thus, the Fresnel coefficients are obtained as

$$\left.\begin{aligned} r_p &= \frac{R_p}{A_{\parallel}} = \frac{n_2\cos\theta_i - n_1\cos\theta_t}{n_2\cos\theta_i + n_1\cos\theta_t} \\ r_s &= \frac{R_s}{A_{\perp}} = \frac{n_1\cos\theta_i - n_2\cos\theta_t}{n_1\cos\theta_i + n_2\cos\theta_t} \\ t_p &= \frac{T_p}{A_{\parallel}} = \frac{2n_1\cos\theta_i}{n_2\cos\theta_i + n_1\cos\theta_t} \\ t_s &= \frac{T_s}{A_{\perp}} = \frac{2n_1\cos\theta_i}{n_1\cos\theta_i + n_2\cos\theta_t} \end{aligned}\right\} \tag{2.37}$$

These equations are described the components of transmitted and reflected waves which are parallel to the plane of incidence and the others those perpendicular to the plane of incidence in terms of those of the incident wave. These two types of waves are independent of one another and separable.

When the wave is linearly polarized with its electric vector perpendicular to the plane of incidence, the polarization mode is called the transverse electric (denoted by *TE*) polarization, orthogonal polarization or *E*-polarized. If the wave is linearly polarized with its magnetic vector perpendicular to the plane of incidence, the polarization mode is called the transverse magnetic (denoted by *TM*) polarization, parallel polarization or *H*-polarized. *TE* and *TM* polarizations are also called the *s* and *p* polarization.

2.5.3. Power Reflectance and Transmittance

To examine how the energy of the incident light is divided among the reflected and transmitted fields, It should be used Poynting vectors $\boldsymbol{S}$ which represents the amount of energy crossed per second a unit area normal to the directions of $\boldsymbol{E}$ and $\boldsymbol{H}$. The power reflectance P_r and transmittance P_t are defined as the ratios of light intensities of the reflected and transmitted light waves to that of the incident light wave. P_r and P_t are also called the reflectivity and transmissivity.

From the (2.1) and (2.32), the light intensity is obtained as

$$S = \frac{c}{4\pi}\sqrt{\varepsilon}\,E^2 = \frac{cn}{4\pi}E^2 . \tag{2.38}$$

Using the amount of energies of the reflected and transmitted wave leaving a unit area of the boundary per second and the amount of energy of the incident wave according to (2.38), the ratios P_r and P_t are given by (2.39) and (2.40) respectively.

$$P_r = \frac{\frac{cn_1}{4\pi}|R|^2 \cos\theta_i}{\frac{cn_1}{4\pi}|A|^2 \cos\theta_i} = \frac{|R|^2}{|A|^2} \tag{2.39}$$

$$P_t = \frac{\frac{cn_2}{4\pi}|T|^2 \cos\theta_t}{\frac{cn_1}{4\pi}|A|^2 \cos\theta_i} = \frac{n_2 \cos\theta_t |T|^2}{n_1 \cos\theta_i |A|^2} \tag{2.40}$$

The law of conservation of energy requires that

$$P_r + P_t = 1 \tag{2.41}$$

For normal incidence (θ_i=0 and consequently θ_t=0), there is no physical distinction between the *s* and *p* polarizations, and the transmissivity and reflectivity are polarization independent:

$$P_r = \frac{|R|^2}{|A|^2} \text{ and } P_t = \frac{n_2|T|^2}{n_1|A|^2} \tag{2.42}$$

Using Eqns. (2.41), (2.42) and Fresnel formulas (2.35) and (2.36)

$$\left.\begin{aligned} P_r &= \left(\frac{n-1}{n+1}\right)^2 \\ P_t &= \left(\frac{2\sqrt{n}}{n+1}\right)^2 \end{aligned}\right\}, n = \frac{n_2}{n_1}. \tag{2.43}$$

As easily seen from (2.43), the smaller the difference in the optical densities of the two media, the less power is carried away by the reflection.

2.5.4. Polarizing Angle (Brewster Angle)

When the reflected and transmitted rays are perpendicular to each other as shown in Fig.2.11, then

$$\theta_i + \theta_t = \frac{\pi}{2}. \tag{2.44}$$

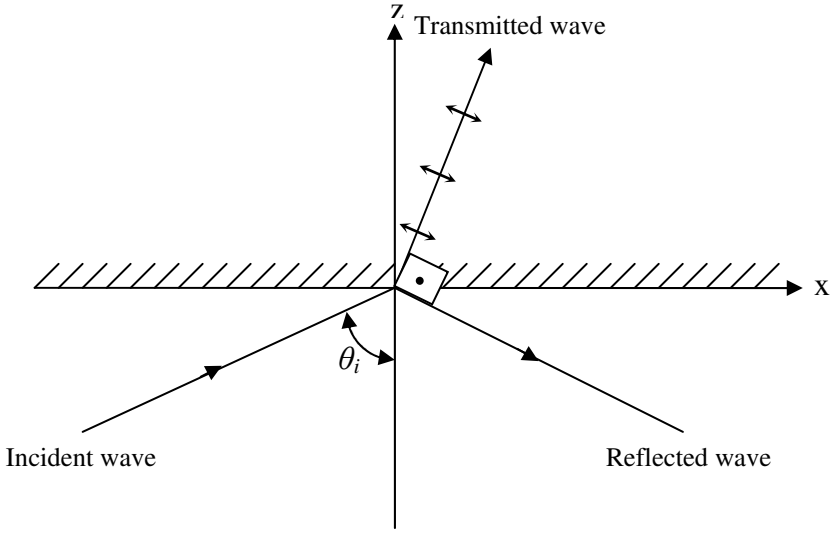

Figure 2.11. An illustration of Polarizing (Brewster's) Angle

The Snell's law and (2.44) gives

$$\left.\begin{aligned} n_2 \cos\theta_i &= n_1 \cos\theta_t \\ n_2 \cos\theta_i &= n_1 \sin\theta_i \\ \tan\theta_i &= n. \end{aligned}\right\} \tag{2.45}$$

Thus, according to the (2.37) the reflection coefficient for *p*-polarized light is zero and the reflected light is entirely composed of the s- linear polarization. In this case, the corresponding angle of incidence light is known as polarizing or Brewster angle. A Brewster-angled reflecting surface thus comprises the simplest linear polarizer.

2.6. Partial Polarization (Degree of Polarization)

The equality $I^2 = Q^2 + U^2 + V^2$ (Eq. 2.18) is valid for the ideal case of a monochromatic plane wave that is completely polarized, where the amplitudes E_{0x} and E_{0y} and the phases φ_x and φ_y are fixed and do not vary with time. This means that the plane wave is emitted from a coherent source. In the case of a natural radiation, the amplitudes and phases fluctuate, since the radiation originates from several sources that do not emit radiation coherently, and since the emission from one source usually has very short coherence times.

Real life usually has a superposition of radiation from several incoherent sources. The polarization state of such sources fluctuates as well. If these fluctuations are random and the different sources emit incoherently while they are not in any way oriented, then the state is called unpolarized. The study of random fluctuations of light is known as the theory of optical coherence. If the fluctuations are not completely random, the radiation is called partially polarized. In these cases the inequality $I^2 > Q^2 + U^2 + V^2$ (Eq. 2.19) is valid, and the statistical theory of random light is needed in order to analysis the effects of polarization.

2.6.1. Statistical Properties of Random Light

An optical wave may be described by a complex wave function such as

$$\boldsymbol{E}(\mathbf{r},t) = \boldsymbol{E}(\boldsymbol{r})exp(j2\pi vt) \tag{2.46}$$

where $\boldsymbol{E}(\boldsymbol{r})$ is the time-independent complex amplitude. A monochromatic wave is an example of coherent light. Its complex amplitude is a deterministic complex function. For random light, the dependence of the wave function on time and position is a random function and not totally predictable.

2.6.1.1. Optical Intensity of Random Light

For an arbitrary optical wave, the average intensity is defined as

$$I(\boldsymbol{r},t) = \langle \left| \boldsymbol{E}(\boldsymbol{r},t) \right|^2 \rangle \tag{2.47}$$

where the quantity $\left| \boldsymbol{E}(\boldsymbol{r},t) \right|^2$ is instantaneous (random) intensity. For coherent light, the averaging operation $\langle . \rangle$ is unnecessary since all trials produce the same wave function. The average intensity in this case is equivalent to

$$I(\boldsymbol{r},t) = \left| \boldsymbol{E}(\boldsymbol{r},t) \right|^2 . \tag{2.48}$$

Statistically stationary waves have average intensities those do not vary with time. In this case, the average intensity ***I(r)*** is only a function of distance from the light source. However, the instantaneous intensity $\left| \boldsymbol{E}(\boldsymbol{r},t) \right|^2$ depends on both position and time. On the other hand, a statistically nonstationary wave has a time-varying intensity (See Figs.2.12)

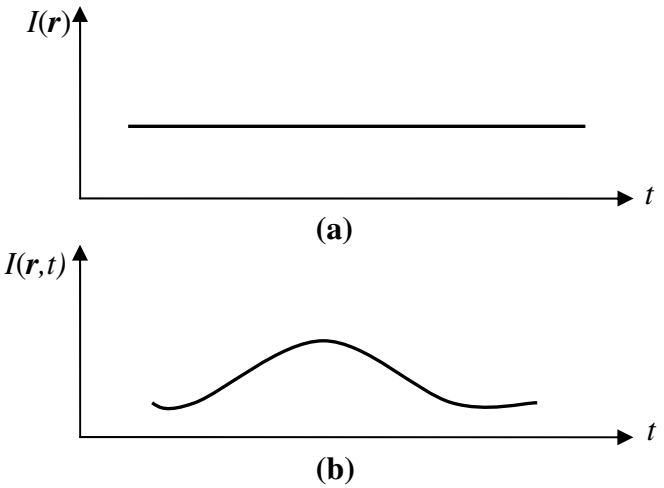

Figure 2.12. a) A Statistically stationary wave. The average intensity does not vary with time
b) An example for statistically nonstationary wave

When the light is nonstationary, the average intensity can usually be determined by the averaging operation over a long time duration as shown in Eqn. (2.49).

$$I(\boldsymbol{r}) = \lim_{T\to\infty} \frac{1}{2T} \int_{-T}^{T} \left|\boldsymbol{E}(\boldsymbol{r},t)\right|^2 dt \tag{2.49}$$

2.6.1.2. Temporal Coherence Function (Autocorrelation Function)

At a fixed position $\boldsymbol{r}$, a random stationary complex wave function $\boldsymbol{E}(\boldsymbol{r},t)$ has a constant intensity as a function of time as shown in Fig.2.12. (a). Since $\boldsymbol{r}$ is fixed, the position dependence may be dropped, so that $\boldsymbol{E}(\boldsymbol{r},t) = \boldsymbol{E}(t)$ and $I(\boldsymbol{r}) = I$.

A quantitative measure of the temporal behavior of the random fluctuations of $\boldsymbol{E}(t)$ can be obtained by defining a statistical average known as the autocorrelation function:

$$\left.\begin{aligned} \mathrm{G}(\tau) &= \langle \boldsymbol{E}^*(t)\boldsymbol{E}(t+\tau)\rangle \\ &= \lim_{T\to\infty} \frac{1}{2T} \int_{-T}^{T} \boldsymbol{E}^*(t)\boldsymbol{E}(t+\tau)dt \end{aligned}\right\} \tag{2.50}$$

In this equations, $\boldsymbol{E}^*(t)$ is the complex conjugate of the random function $\boldsymbol{E}(t)$ and τ is the time delay. Since $G(\tau)$ has a Hermitian symmetry, $G(-\tau) = G^*(\tau)$ and for $\tau = 0$ the intensity, defined by (2.47) is equal to $G(\tau)$,

$$I = G(0). \tag{2.51}$$

2.6.1.3. Degree of Temporal Coherence

Complex degree of temporal coherence is given by the normalized autocorrelation function,

$$g(\tau) = \frac{G(\tau)}{G(0)} = \frac{\langle \boldsymbol{E}^*(t)\boldsymbol{E}(t+\tau)\rangle}{\langle \boldsymbol{E}^*(t)\boldsymbol{E}(t)\rangle}. \tag{2.52}$$

The absolute value, which is a measure of the degree of correlation between $\boldsymbol{E}(t)$ and $\boldsymbol{E}(t+\tau)$ cannot exceed unity,

$$0 \le \left| g(\tau) \right| \le 1. \tag{2.53}$$

For a deterministic and monochromatic light such as $\boldsymbol{E}(t) = \boldsymbol{E}\, exp(j2\pi v_0 t)$, the amplitude $\boldsymbol{E}$ is a constant, then (2.52) gives $g(\tau) = exp(j2\pi v_0 \tau)$ and thus $\left| g(\tau) \right| = 1$ for all times delays τ and $\boldsymbol{E}(t)$ and $\boldsymbol{E}(t+\tau)$ are completely correlated.

However, in general, for an arbitrary light, $\left| g(\tau) \right|$ decreases from the largest value $\left| g(0) \right| = 1$ with time delay τ and drops to *1/2* or *1/e* for $\tau = \tau_c$ where

$$\tau_c = \int_{-\infty}^{\infty} \left| g(\tau) \right|^2 d\tau \tag{2.54}$$

known as the coherence time and used as a measure of the memory time of the fluctuations. The fluctuations have high correlation for $\tau < \tau_c$ and low correlation for longer time delays $\tau > \tau_c$ (see Fig.2.13).

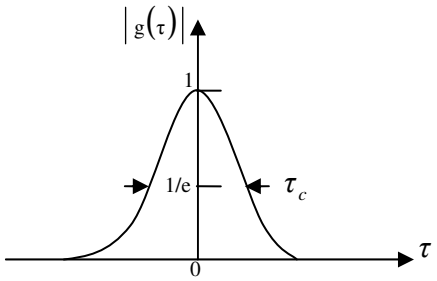

Figure 2.13. An example for the relation between the magnitude of temporal coherence $\left| g(\tau) \right|$ and coherence time τ_c

The distance $c\tau_c$ is referred as the coherence length. Since the coherence time of monochromatic light is infinite its coherence length also infinite. Effectively coherent light is the light with long coherent length compared with all optical path-length differences belong to it.

2.6.2. Coherency Matrix and Degree Of Polarization

The theory of partial polarization is based on characterizing the components of the wave vector by their correlations and cross-correlations. Each component, that is

generally random, characterized by its temporal coherence function. For light described by a *p*-polarized plane wave traveling in the *z*-direction, these functions related to components $\boldsymbol{E_x}(t)$ and $\boldsymbol{E_y}(t)$ are

$$\left.\begin{aligned} \mathrm{G}_{xx}(\tau) &= \langle \boldsymbol{E_x}^{*}(t)\boldsymbol{E_x}(t+\tau)\rangle, \\ \mathrm{G}_{yy}(\tau) &= \langle \boldsymbol{E_y}^{*}(t)\boldsymbol{E_y}(t+\tau)\rangle. \end{aligned}\right\} \tag{2.55}$$

Similarly, the cross-correlation function of $\boldsymbol{E_x}(t)$ and $\boldsymbol{E_y}(t)$ is given as

$$\mathrm{G}_{xy}(\tau) = \langle \boldsymbol{E_x}^{*}(t)\boldsymbol{E_y}(t+\tau)\rangle . \tag{2.56}$$

The normalized function similar to the (2.52),

$$g_{xy}(\tau) = \frac{G_{xy}(\tau)}{\sqrt{G_{xx}(0)G_{yy}(0)}} \tag{2.57}$$

is known as the cross-correlation coefficient of $\boldsymbol{E_x}^{*}(t)$ and $\boldsymbol{E_y}(t+\tau)$. The magnitude of $g_{xy}(\tau)$ satisfies the inequality,

$$0 \le \left| \mathrm{g}_{\mathrm{xy}}(\tau) \right| \le 1. \tag{2.58}$$

If the two components are completely correlated at all times, then $\left| \mathrm{g}_{\mathrm{xy}}(\tau) \right| = 1$ and if they are uncorrelated for all times, $\left| \mathrm{g}_{\mathrm{xy}}(\tau) \right| = 0$

For quasi-monochromatic light, all dependences on τ for both correlation and autocorrelation functions are approximately of the form $exp(j2\pi\nu_0\tau)$, so that the polarization properties can be described by their values when $\tau = 0$. According to the (2.51), $\mathrm{G}_{xx}(0) = I_x$ and $\mathrm{G}_{yy}(0) = I_Y$ are real numbers representing the intensities of the *x* and *y* components. $\mathrm{G}_{xy}(0)$ and $\mathrm{G}_{yx}(0) = \mathrm{G}^{*}_{xy}(0)$ are complex numbers. These four variables may be written in the form of a *2x2* Hermittian matrix,

$$\mathbf{G} = \begin{pmatrix} \mathrm{G}_{xx} & \mathrm{G}_{xy} \\ \mathrm{G}_{yx} & \mathrm{G}_{yy} \end{pmatrix} \tag{2.59}$$

G is called the coherency matrix, used to describe the polarization of the wave where the off-diagonal elements are the cross-correlations values at $\tau = 0$. The trace of the matrix, $Tr\mathbf{G}=I_x+I_y$, is the total intensity $\boldsymbol{I}$.

It is also possible to write the coherency matrix in terms in terms of the Jones vectors, $J = \begin{pmatrix} E_x \\ E_y \end{pmatrix}$,

$$\left.\begin{aligned} \langle J^* J^t \rangle &= \left\langle \begin{pmatrix} E_x^* \\ E_y^* \end{pmatrix} \begin{pmatrix} E_x & E_y \end{pmatrix} \right\rangle \\ &= \begin{pmatrix} \langle E_x^* E_x \rangle & \langle E_x^* E_y \rangle \\ \langle E_y^* E_x \rangle & \langle E_y^* E_y \rangle \end{pmatrix} = \mathbf{G} \end{aligned}\right\} \tag{2.60}$$

where t denotes the transpose of a matrix.

The Jones vector of incident light J_{in} is transformed by the optical system such as polarizer with the rule,

$$J_{out} = TJ_{in} \tag{2.61}$$

where T is a *2x2* Jones matrix characterizing the device. Using (2.60) and (2.61), the coherency matrix of partially polarized incident light $\mathbf{G}_{\mathrm{in}}=\langle J_{in}^* J_{in}^t \rangle$ is transformed to,

$$\left.\begin{aligned} \mathbf{G}_{\mathrm{out}} &= \langle J_{out}^* J_{out}^t \rangle \\ &= \langle (TJ_{in})^* (TJ_{in})^t \rangle \\ &= T^* \langle J_{in}^* J_{in}^t \rangle T^t \\ &= T^* \mathbf{G}_{\mathrm{in}} T.^t \end{aligned}\right\} \tag{2.62}$$

In the case of unpolarized light, the two components E_x and E_y have the same intensity $I_x = I_y = \boldsymbol{I/2}$, and there are no correlation between them, then the coherency matrix is,

$$\mathbf{G} = \frac{\boldsymbol{I}}{2}\begin{pmatrix} 1 & 0 \\ 0 & 1 \end{pmatrix}. \tag{2.63}$$

Unpolarized light becomes linearly polarized at the output when passed through a polarizer. However, it can be shown that (2.63) is unaffected from the rotation of the coordinate system, so that incident unpolarized light to a polarization rotator also unpolarized at the output. In such situations, the cross-correlation coefficient magnitude $\left|g_{xy}\right| = 0$ and the intensities always satisfy the equality $I_x = I_y = \boldsymbol{I/2}$.

When $\left|g_{xy}\right| = 1$, E_x and E_y are perfectly correlated, then light is said to be completely polarized. Using $g_{xy} = G_{xy} \Big/ \sqrt{I_x I_y}$, the coherency matrix for polarized light is given as,

$$\mathbf{G} = \begin{pmatrix} I_x & \left[I_x I_y\right]^{1/2} e^{j\varphi} \\ \left[I_x I_y\right]^{1/2} e^{-j\varphi} & I_y \end{pmatrix} \tag{2.64}$$

where φ is the argument of g_{xy}. E_x and E_y are may be defined as $\sqrt{I_x}$ and $\sqrt{I_y}e^{j\varphi}$, then the coherency matrix takes the form,

$$\mathbf{G} = \begin{pmatrix} E_x^* E_x & E_x^* E_y \\ E_y^* E_x & E_y^* E_y \end{pmatrix} = J^* J^t \tag{2.65}$$

which is the form of the coherency matrix of a coherent wave.

The coherency matrices for different states of polarization can be obtained by using the Jones vectors. Some examples are given in Table 2.5.

Table 2.5. Coherency matrices for different states of polarization

Linearly polarized in the *y* direction	$\mathbf{G} = \boldsymbol{I}\begin{pmatrix} 0 & 0 \\ 0 & 1 \end{pmatrix}$	Linearly polarized in the x direction	$\mathbf{G} = \boldsymbol{I}\begin{pmatrix} 1 & 0 \\ 0 & 0 \end{pmatrix}$
Right circularly polarized wave	$\mathbf{G} = \frac{\boldsymbol{I}}{2}\begin{pmatrix} 1 & j \\ -j & 1 \end{pmatrix}$	Left circularly polarized wave	$\mathbf{G} = \frac{\boldsymbol{I}}{2}\begin{pmatrix} 1 & -j \\ j & 1 \end{pmatrix}$

There exist different approaches to estimate the degree of polarization of light. One of them is a measurement using the coherency matrices. A quasi-monochromatic wave may be defined as the sum of two waves, which are one completely polarized and one completely unpolarized. Hence, the coherency matrix of a quasi-monochromatic wave may be also expressed as $\mathbf{G} = G_1 + G_2$, where G_1 and G_2 are the coherency matrices of the polarized and unpolarized waves. Degree of polarization is may be defined as the ratio of the intensity of the completely polarized part $I_{pol}=TrG_2$ to the total intensity $\boldsymbol{I}=Tr\mathbf{G}$. The coherency matrix of polarized part G_2 is may be given as,

$$G_2 = \begin{pmatrix} \frac{1}{2}\left[\left(\mathrm{G}_{xx} - \mathrm{G}_{yy}\right) + \sqrt{\left(\mathrm{G}_{xx} + \mathrm{G}_{yy}\right)^2 - 4|\mathbf{G}|}\right] & \mathrm{G}_{xy} \\ \mathrm{G}_{yx} & \frac{1}{2}\left[\left(\mathrm{G}_{yy} - \mathrm{G}_{xx}\right) + \sqrt{\left(\mathrm{G}_{xx} + \mathrm{G}_{yy}\right)^2 - 4|\mathbf{G}|}\right] \end{pmatrix} \quad (2.66)$$

which can be calculated from $\mathbf{G} = G_1 + G_2$ (Born and Wolf 1986). The intensity of the polarized part then,

$$\left.\begin{aligned} I_{pol} &= TrG_2 = \sqrt{\left(\mathrm{G}_{xx} + \mathrm{G}_{yy}\right)^2 - 4|\mathbf{G}|} \\ &= \left[(Tr\mathbf{G})^2 - 4\,det\,\mathbf{G}\right]^{1/2} \end{aligned}\right\}. \quad (2.67)$$

Thus, now, using $g_{xy} = G_{xy} \Big/ \sqrt{I_x I_y}$, (2.64) and (2.67), degree of polarization can be calculated in the form as below:

$$p = \frac{I_{pol}}{\boldsymbol{I}} = \frac{TrG_2}{Tr\mathbf{G}} = \left\{1 - \frac{4\,det\,\mathbf{G}}{(Tr\mathbf{G})^2}\right\}^{1/2}$$
$$= \left\{1 - 4\left[\frac{I_x I_y}{(I_x + I_y)^2}\right]\left(1 - \left|g_{xy}\right|^2\right)\right\}^{1/2} \tag{2.68}$$

Since p is a definition in terms of determinant and trace of a matrix which are invariant to unitary transformations, it is invariant to rotation of the coordinate system (Saleh 1991).

Degree of polarization p in (2.68) takes its minimum value p=0 for unpolarized light ($\left|g_{xy}\right| = 0$, $I_x = I_y$ and then p=0) and maximum value p=1 when the light is completely polarized ($\left|g_{xy}\right| = 1$, $\left(1 - \left|g_{xy}\right|^2 = 0\right)$ and then p=1). Thus, as expected, p satisfies the inequality

$$0 \le p \le 1. \tag{2.69}$$

For a wave which is mutually incoherent with coherency matrix as,

$$\mathbf{G} = \begin{pmatrix} \mathrm{G}_{xx} & 0 \\ 0 & \mathrm{G}_{yy} \end{pmatrix} = \begin{pmatrix} I_x & 0 \\ 0 & I_y \end{pmatrix} \tag{2.70}$$

since G_{xy}= G_{yx}=0, and then $det\mathbf{G}$=$G_{xx}G_{yy}$=I_xI_y, the degree of polarization p takes the form,

$$p = \left\{1 - \frac{4\,det\,\mathbf{G}}{(Tr\mathbf{G})^2}\right\}^{1/2} = \left\{1 - \frac{4I_x I_y}{(I_x + I_y)^2}\right\}^{1/2} = \left|\frac{(I_x - I_y)}{(I_x + I_y)}\right|. \tag{2.71}$$

One of the expressions of the degree of polarization is used the Stokes vectors. The Stokes vector of any quasi-monochromatic light can be separated into two parts:

$$S = \begin{pmatrix} I \\ Q \\ U \\ V \end{pmatrix} = \begin{pmatrix} I - \sqrt{Q^2 + U^2 + V^2} \\ 0 \\ 0 \\ 0 \end{pmatrix} + \begin{pmatrix} \sqrt{Q^2 + U^2 + V^2} \\ Q \\ U \\ V \end{pmatrix} \tag{2.72}$$

where the left of the sum represents the Stokes vector of a fully unpolarized part and the right hand side represents the Stokes vector of completely polarized part of light. Thus, the degree of polarization is defined as

$$p = \frac{\left(Q^2 + U^2 + V^2\right)^{1/2}}{I}. \tag{2.73}$$

CHAPTER 3

POLARIZATION BY SCATTERING

3.1. Introduction

A small particle, which is interposed into the light, can cause several effects such as absorption, elastic scattering, and extinction. By absorption, the particle converts some of the energy contained in the light into other forms of energy. The reduction of the incidence energy by an amount equal to the sum of absorption and scattering is known as extinction (Van de Hulst 1981). A completely homogeneous material can be scattered light only in the direction of incident light wave (Boyd 2003). These types of scattering are known as coherent forward scattering.

Scattering, generally, is classified into two types, spontaneous and stimulated light scattering. If the optical properties of the medium are unaffected from the incident light, scattering is called spontaneous light scattering. Stimulated light scattering occurs when the intensity of the incident light is sufficiently large to change the optical properties of the material system.

Light scattering occurs only when the medium has inhomogeneous optical properties. To get a picture of the physical process, it is useful to subdivide the particle of the medium into small regions. Applying an electromagnetic wave induces dipole moments in each region, which themselves emit electromagnetic radiation. For example, if the volume elements of a material, such as *dV1* and *dV2* differ in the density, so the number of molecules in volume elements not equal, then the fields scattered by these two elements will not be interference with incidence light exactly, causing scattering in different angles. Scattering can involve change in polarization, and can occur in all types of materials.

Consider an observer (dedector) in the far-field zone, which means that the distance to the scattering object r is large compared to the wavelength and any linear dimension of the scattering object. The scattering event is depicted conceptually in Fig. 3.1, where an incident plane wave is transformed, i.e., scattered, by a particle into a spherical wave.

The intensity I^{sca} of the scattered light measured at a distance r from the interaction region, assuming linear positive correlation to the intensity I_0 of the incident light, is given as,

$$I^{sca} = \frac{I_0 F(\theta,\varphi)}{k^2 r^2} \tag{3.1}$$

where $F(\theta,\varphi)$ is a dimensionless function of the direction and $k=2\pi/\lambda$ is the wave number. When this function is divided by

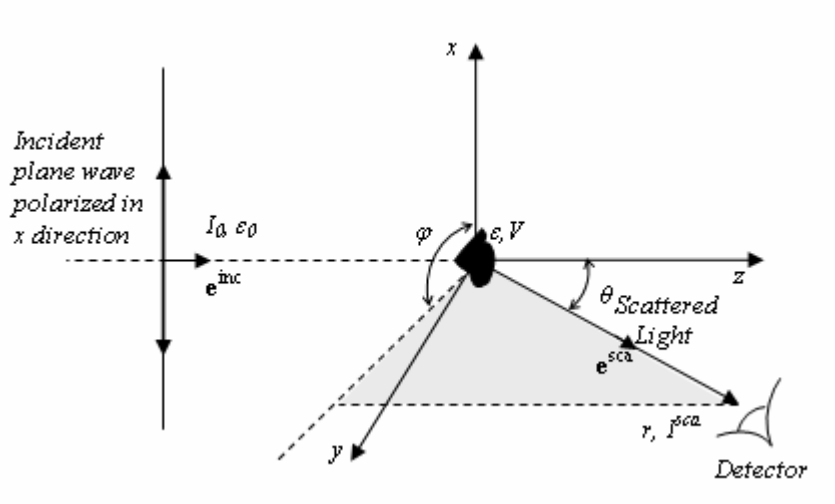

Figure 3.1. Geometry used to define the scattering

$$k^2 C_{sca} \tag{3.2}$$

the phase function is obtained where

$$C_{sca} = \frac{1}{k^2}\int F(\theta,\varphi)d\Omega \tag{3.3}$$

is the cross section of the particle for scattering. $d\Omega = \sin\theta\, d\theta\, d\varphi$ is the element of solid angle and the integral is taken over all directions.

The law of conservation of energy requires that

$$C_{ext} = C_{sca} + C_{abs} \tag{3.4}$$

where C_{ext} and C_{abs} are the cross sections of the particle for extinction and absorption respectively.

The constants $Q_{ext} = C_{ext}/A$, $Q_{sca} = C_{sca}/A$, and $Q_{abs} = C_{abs}/A$ are given as the dimensionless efficiency factors for extinction, scattering, and absorption respectively where *A* is the geometrical cross section of the particle.

In our study, we are interested in diffuse scattering from dielectric nonspherical scatterers in optical films those very large in size compared to the wavelength. We especially aimed to obtain the polarization effects of scatterers aligned with fixed orientation on surfaces of the dielectric film.

3.2. Amplitude Scattering Matrix

Consider an observer (dedector) in the far-field zone, which means that the distance to the scattering object *r* is large compared to the wavelength and any linear dimension of the scattering object.

The direction of scattered light is parameterized by a polar (in the plane of incidence) angle θ and azimuthal (out-of plane of incidence) angle φ relative to the *y*-*z* plane.

As described in previous chapter, the scattered electromagnetic field in the far field is can be related to the incident field by the amplitude scattering matrix *S* as

$$\begin{pmatrix} E_p^{sca} \\ E_s^{sca} \end{pmatrix} = \frac{e^{-ik(r-z)}}{ikr} \begin{pmatrix} S_2 & S_3 \\ S_4 & S_1 \end{pmatrix} \begin{pmatrix} E_p^{inc} \\ E_s^{inc} \end{pmatrix} \tag{3.5}$$

where E_s^{inc} and E_p^{inc} are the amplitudes of the vertical and horizontal components of the incident plane parallel wave transformed to the scattering plane, and E_s^{sca} and E_p^{sca} are the vertical and horizontal components of the scattered spherical wave. The amplitude scattering matrix provides a complete description of the scattering pattern in the far-field zone. The elements S_j are the complex amplitude functions described the scattering in any direction and all are functions of θ and φ. The intensity relationship can be expressed using the Stokes-Mueller representation defined by (2.15).

Knowledge of the these scattering matrix elements suffices for calculation the intensity and polarization of scattered light in addition to absorption, extinction, radiation pressure and the total scattering cross sections of the particle.

3.3. Scattering Diagram for Polarized Light

The exact relations indicating how the intensity I^{sca} and state of polarization of the scattered light depend on the intensity I^{inc} and state of polarization of the incident light given by equation,

$$I^{sca}\left(r\mathbf{e}^{sca}\right)=\frac{1}{k^2r^2}\boldsymbol{M}\left(\mathbf{e}^{inc},\mathbf{e}^{sca}\right)I^{inc}. \tag{3.6}$$

The phase matrix $\boldsymbol{M}$ describes the transformation of the Stokes vector of the incident wave defined in Sec.2.3.2 into that of the scattered wave for scattering directions $\mathbf{e}^{sca}$ away from the incidence direction $\mathbf{e}^{inc}$. The transformation matrix $\boldsymbol{M}$ is a *4x4* matrix and can be written in terms of the amplitude matrix elements having the dimension of area. Its elements are real for single particles. The phase matrix also depends on $\mathbf{e}^{sca}$ and $\mathbf{e}^{inc}$ for all polar and azimuthal angels of incidence and scattered lights.

Using Eq.2.16, Eq.3.5 becomes

$$\begin{pmatrix} I \\ Q \\ U \\ V \end{pmatrix}=\frac{1}{k^2r^2}\begin{pmatrix} m_{11} & m_{12} & m_{13} & m_{14} \\ m_{21} & m_{22} & m_{23} & m_{24} \\ m_{31} & m_{32} & m_{33} & m_{34} \\ m_{41} & m_{42} & m_{43} & m_{44} \end{pmatrix}\begin{pmatrix} I_0 \\ Q_0 \\ U_0 \\ V_0 \end{pmatrix} \tag{3.7}$$

where I, Q, U, and V are the Stokes parameters of scattered light, and I_0, Q_0, U_0, and V_0 are the corresponding parameters of the incident light.

3.4. Scattering from Dielectric Spheres

Gustav Mie in 1908 published a solution to the problem of light scattering by homogeneous spherical particles of any size. Mie theory describes the scattering of light by particles. Optical dielectric filters may have particles with refractive index m_{par} that differs from the refractive index of the surrounding medium m_{med} of the dielectric film. Such particles yield a strong net source of scattered radiation.

Scattering can be divided into surface/interface scattering and volume scattering. While surface scattering largely dominates both substrate and thin film scattering losses, in particular cases and applications, volume scattering can constitute the main scattering source.

Surface scattering is defined as the scattering which takes place only on the border surface between two different but homogeneous media (see Fig.3.3).

We are interested in sphere of a non-absorbing material that the electrical conductivity is zero (dielectric) and the refractive index m_{par} is a real constant. A real value of m_{par} means no absorption (Q_{abs}=0), so that Q_{sca}= Q_{ext}.

Mie's classical solution is described in terms of two parameter; the magnitude of refractive index expressed as the ratio of the for particle and medium

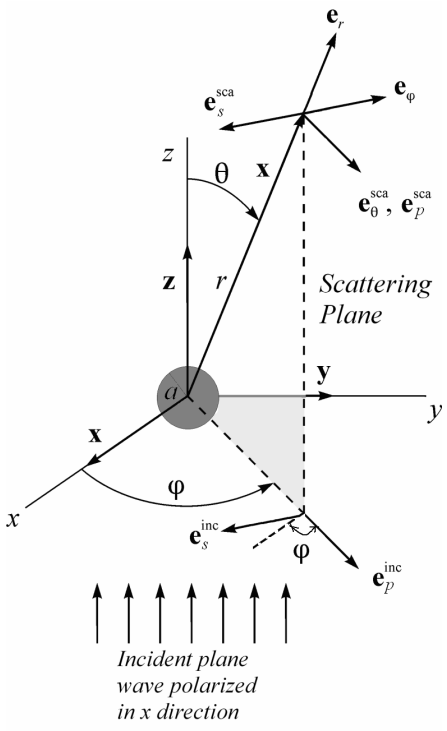

Figure 3.2.Geometry used to define the scattering from a spherical particle

$$m = \frac{m_{par}}{m_{med}} \tag{3.8}$$

and the size of the surface of refractive index mismatch expressed as a size parameter

$$x = \frac{2\pi a m_{med}}{\lambda} . \tag{3.9}$$

A Mie theory calculation yields the efficiency of scattering, the scattering coefficient related to the product of scatterer number density, and the cross-sectional area of scattering, C_{sca} (WEB_7 2007).

It is assumed that, as illustrated in Fig. 3.2, a spherical particle with radius a much larger then the wavelength of incident optical field $\boldsymbol{E}^{inc}$, located at the origin of a coordinate system. $\boldsymbol{E}^{inc}$ is a linear monochromatic plane wave polarized in x- direction and propagates in z direction.

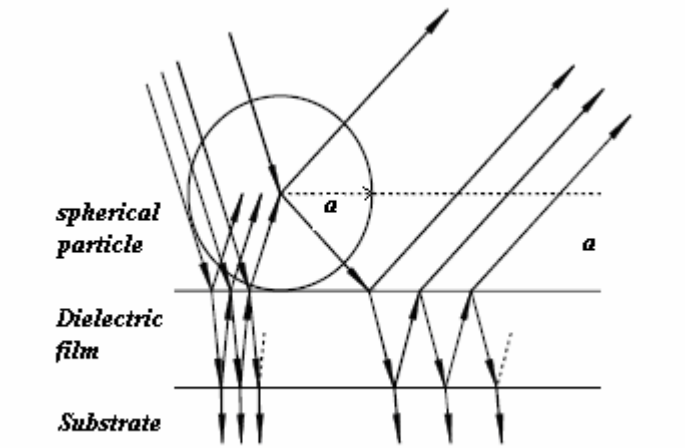

Figure 3.3. A schematic representation for light scattering from a sphere on a dielectric film (An example of surface scattering)

The extinction and scattering efficiencies of a sphere may be written as Eqns. (3.11) where the coefficients a_n and b_n are referred to as Mie scattering coefficients and are functions of x and m.

$$\left.\begin{aligned} Q_{ext} &= \frac{2}{x^2}\sum_{n=1}^{\infty}(2n+1)\Re(a_n+b_n) \\ Q_{sca} &= \frac{2}{x^2}\sum_{n=1}^{\infty}(2n+1)\left(|a_n|^2+|b_n|^2\right) \end{aligned}\right\} \tag{3.10}$$

The scattering coefficient

$$\mu_{sca} = \rho_{sca} C_{sca} \tag{3.11}$$

describes a medium containing many scattering particles at a concentration described as a volume density ρ_{sca}. The scattering coefficient is essentially the cross-sectional area per unit volume of medium.

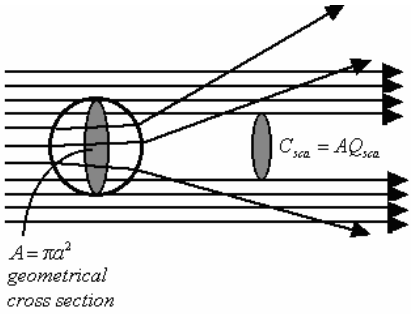

Figure 3.4. Representation of geometrical cross section and scattering cross section for a spherical partice

3.5. Reduced Form of the Transformation Matrix

By defining the real numbers for $j,k = 1, 2, 3, 4$;

$$\left.\begin{aligned} N_k &= S_k S_k^* = |S_k|^2 \\ S_{kj} = S_{jk} &= \frac{1}{2}\left(S_j S_k^* + S_k S_j^*\right) \\ -D_{kj} = D_{jk} &= \frac{i}{2}\left(S_j S_k^* - S_k S_j^*\right) \end{aligned}\right\} \tag{3.12}$$

The transformation matrix $\boldsymbol{M}$ has the form,

$$\boldsymbol{M} = \begin{pmatrix} \frac{1}{2}(N_2 + N_3 + N_4 + N_1) & \frac{1}{2}(N_2 - N_3 + N_4 - N_1) & S_{23} + S_{41} & -D_{23} - D_{41} \\ \frac{1}{2}(N_2 + N_3 - N_4 - N_1) & \frac{1}{2}(N_2 - N_3 - N_4 + N_1) & S_{23} - S_{41} & -D_{23} + D_{41} \\ S_{24} + S_{31} & S_{24} - S_{31} & S_{21} + S_{34} & -D_{21} + D_{34} \\ D_{24} + D_{31} & D_{24} - D_{31} & D_{21} + D_{34} & S_{21} - S_{34} \end{pmatrix}. \quad (3.13)$$

Although $\boldsymbol{M}$ has 16 elements, it contains 7 independent constants, resulting from the 8 constants in the S's minus an irrelevant phase. Thus, there are 9 relations between the 16 coefficients.

If $I_p = E_p^{sca} E_p^{sca*}$ and $I_s = E_s^{sca} E_s^{sca*}$ are used instead of I and Q as were mentioned in Section 2.3.2., the simpler but less symmetric form can be defined by

$$\begin{pmatrix} I_p \\ I_s \\ U \\ V \end{pmatrix} = \frac{1}{k^2 r^2} \boldsymbol{M}' \begin{pmatrix} I_{p0} \\ I_{s0} \\ U_0 \\ V_0 \end{pmatrix}. \quad (3.14)$$

Here I_{p0} and I_{s0} are the intensities of incident light those parallel and perpendicular to the plane of scattering and

$$\boldsymbol{M}' = \begin{pmatrix} N_2 & N_3 & S_{23} & -D_{23} \\ N_4 & N_1 & S_{41} & -D_{23} + D_{41} \\ 2S_{24} & 2S_{31} & S_{21} + S_{34} & -D_{21} + D_{34} \\ 2D_{24} & 2D_{31} & D_{21} + D_{34} & S_{21} - S_{34} \end{pmatrix}. \quad (3.15)$$

These most general formulas are hardly needed for practical studies. Spherical particles, for all types of polarization of the incident light, have $S_3(\theta) = S_4(\theta) = 0$ in the amplitude scattering matrix,

$$S_{sph} = \begin{pmatrix} S_2(\theta) & 0 \\ 0 & S_1(\theta) \end{pmatrix} \quad (3.16)$$

By using (3.16) in the (3.5) the relation between components of incident and scattered light in the scattering plane for the spherical particle becomes,

$$\begin{pmatrix} E_p^{sca} \\ E_s^{sca} \end{pmatrix} = \frac{e^{-ik(r-z)}}{ikr} \begin{pmatrix} S_2(\theta) & 0 \\ 0 & S_1(\theta) \end{pmatrix} \begin{pmatrix} E_p^{inc} \\ E_s^{inc} \end{pmatrix} \tag{3.17}$$

where θ is the scattering angle. Eq. (3.17) gives the two relations:

$$E_p^{sca} = S_2(\theta) \frac{e^{-ik(r-z)}}{ikr} E_p^{inc} \tag{3.18}$$

$$E_s^{sca} = S_1(\theta) \frac{e^{-ik(r-z)}}{ikr} E_s^{inc} \tag{3.19}$$

Now, the intensities of light can be calculated for parallel and perpendicular to the scattering plane as (3.20) and (3.21) respectively.

$$I_p = \frac{|S_2(\theta)|^2}{k^2 r^2} I_{p0} \tag{3.20}$$

$$I_s = \frac{|S_1(\theta)|^2}{k^2 r^2} I_{s0} \tag{3.21}$$

In this case the matrix ***M'*** has very simple form

$$\boldsymbol{M}' = \begin{pmatrix} N_2 & 0 & 0 & 0 \\ 0 & N_1 & 0 & 0 \\ 0 & 0 & S_{21} & -D_{21} \\ 0 & 0 & D_{21} & S_{21} \end{pmatrix}, \tag{3.22}$$

That is only 3 independent parameters yield since there is only one interrelation:

$$S_{21}^2 + D_{21}^2 = N_2 N_1 . \tag{3.23}$$

In this case, all of the transformation equations for the stokes parameters are

$$\left.\begin{aligned} I_p &= |A_2|^2 I_{p0} \\ I_s &= |A_1|^2 I_{s0} \\ U &= |A_1||A_2|(U_0 \cos\delta - V_0 \sin\delta) \\ V &= |A_1||A_2|(U_0 \cos\delta + V_0 \cos\delta) \end{aligned}\right\} \tag{3.24}$$

where $A_1 = S_1(\theta)e^{-ik(r-z)}/ikr$, $A_2 = S_2(\theta)e^{-ik(r-z)}/ikr$ and δ is the phase difference between A_1 and A_2. When the incident light is linearly polarized in one of the main planes, it remains in the same polarization state in the corresponding plane and the two upper transformation equations are needed to be analyzed. Now, the scattering polarization can be defined as normalized form

$$p = \frac{I_p - I_s}{I_p + I_s} \tag{3.25}$$

The polarization variation for scattered light with scattering angle shown in Fig.3.5 when the scatterer is a small dielectric sphere (smaller than wavelength of the light) and in Fig.3.6 when the scatterer is larger than incident wavelength of the light.

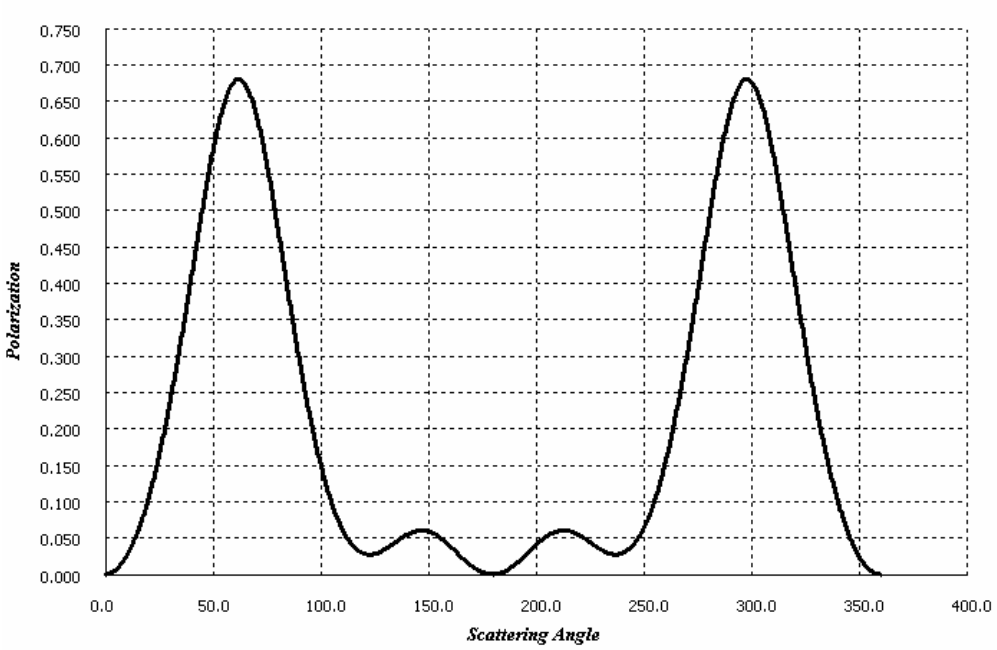

Figure 3.5. The variation of polarization of scattered light for a 100 nm diameter dielectric sphere with a refractive index m = 1.59

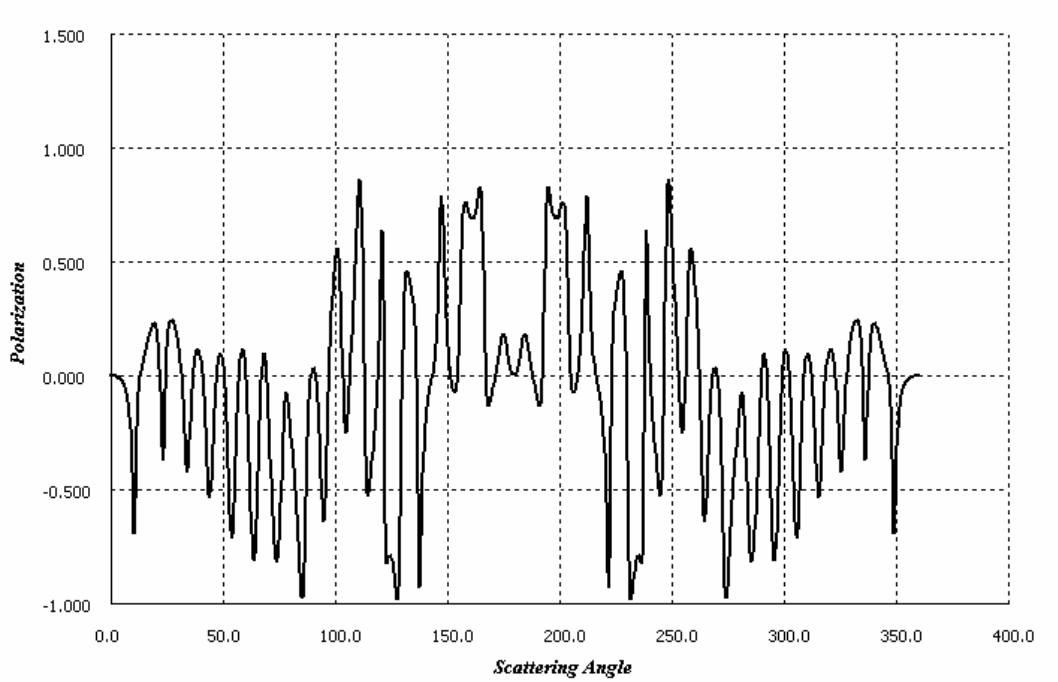

Figure 3.6. The variation of polarization of scattered light for a 2 μm diameter dielectric sphere with a refractive index m = 1.45

In the point (r,θ,φ), in the far-field (see Fig.3.2), the total scattered intensity defined in (3.1) and (3.6), is can be given in the form by

$$I^{sca} = \left[i_1(\theta)\sin^2\varphi + i_2(\theta)\cos^2\varphi\right]\frac{I_0}{k^2r^2} \tag{3.26}$$

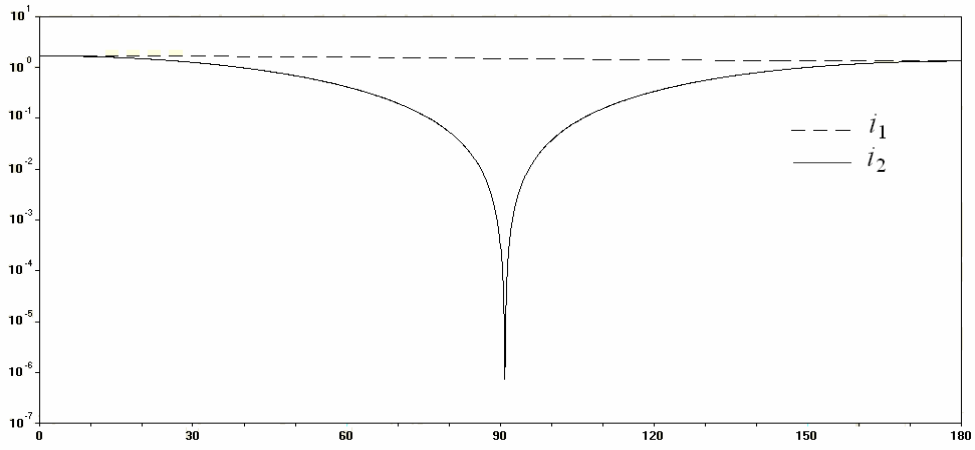

Figure 3.7. The variation of far-field scattered intensities i_1 and i_2 for a 100 nm diameter dielectric sphere with a refractive index m= 1.59

where $i_1(\theta) = |S_1(\theta)|^2$ and $i_2(\theta) = |S_2(\theta)|^2$ are far-field scattered intensities, for the perpendicular and parallel polarization respectively. Fig.3.7. shows an example of the far-field scattered intensities i_1 and i_2 calculated as a function of the scattering angle θ. The calculation is based on a 100 nm diameter dielectric sphere with a refractive index m = 1.59.

The variation of the far-field scattered intensities and polarization at small scattering angels for a large dielectric sphere with radius 1μm are shown in Fig.3.8 and Fig.3.9. respectively.

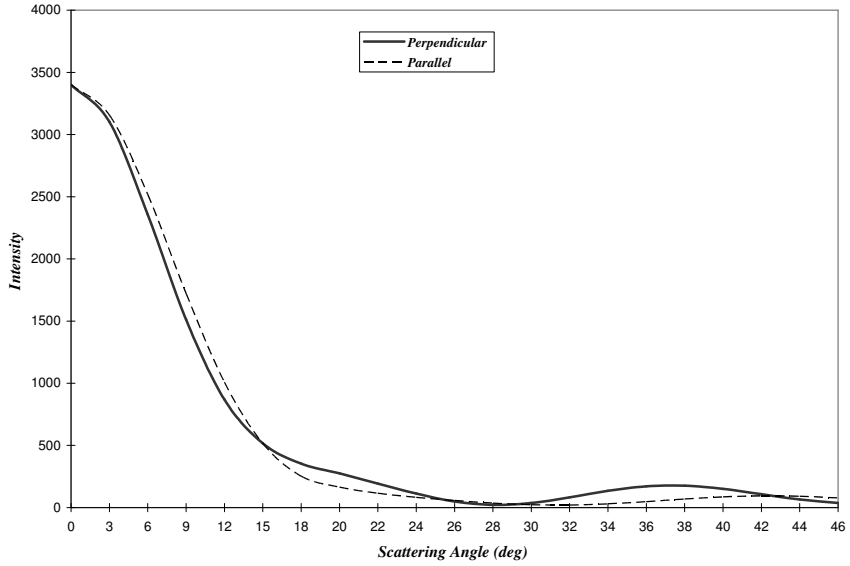

Figure 3.8.The variation of far-field scattered intensities i_1 and i_2 with scattering angle. The scatterer is a 2μm diameter dielectric sphere with a refractive index m= 1.45

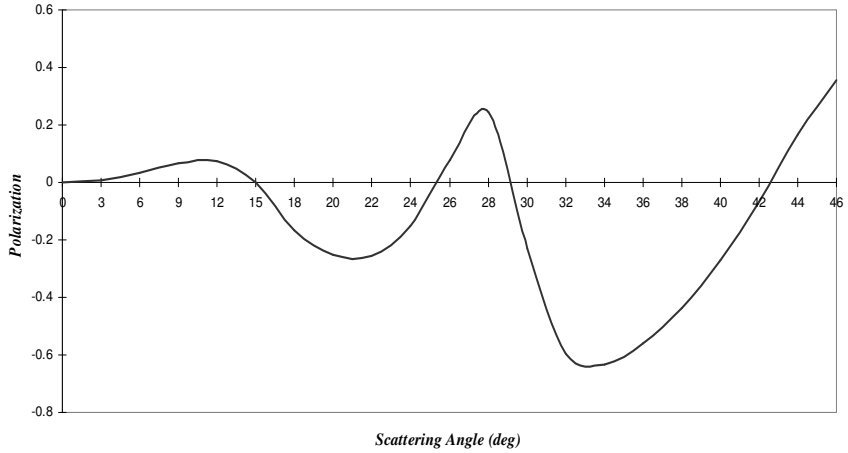

Figure 3.9.The variation of polarization with scattering angle. The Scatterer is a dielectric sphere with 2μm diameter (very large compared to the wavelength) has a refractive index m= 1.45

CHAPTER 4

LIGHT SCATTERING FROM NONSPHERICAL SCATTERERS

4.1. Introduction

There is a long interest in light scattering computations for nonspherical particles in addition to spherical scatterers. The assumption in Mie theory calculations is that the particle shape geometry is spherical and the refractive index is isotropic. Since these restrictions, Mie theory can not be used for analyzing scattering from the nonspherical scatterers.

The three-dimensional objects can be defined as superellipsoid (superquadratic ellipsoid) represented by the product of two superquadratic curves. The exact form, the generalization of the ellipsoid, is given by the equation (Wriedt 2002)

$$\left.\begin{aligned}\left[\left(\frac{x}{a}\right)^{2/e}+\left(\frac{y}{b}\right)^{2/e}\right]^{e/n}+\left(\frac{z}{c}\right)^{2/n}&=1\\ x=a\cos^{n}(\vartheta)\cos^{e}(\varphi)&\\ y=b\cos^{n}(\vartheta)\sin^{e}(\varphi)&\\ z=c\sin^{n}(\varphi)&\end{aligned}\right\},\ \vartheta:[-\pi/2,\pi/2],\ \varphi:[-\pi,\pi] \tag{4.1}$$

n and *e* represent the north-south and the east-west roundedness respectively. For convex shapes these two parameters are bounded: $0<\{e,n\}<2$. The bounds in *x, y, z* are given by the parameters *a, b, c*.

There are various methods available to compute light scattering by nonspherical particles. In volume-based method the computer time is rather long since the whole volume of a scatterer is discretized. The discrete dipole approximation (DDA) (Ayrancı et al. 2007), the volume integral equation method (VIEM) and the finite difference time domain method (FDTD) (Wriedt 1998) are general volume integral equation techniques

used to calculate scattering and absorption of electromagnetic waves by particles of arbitrary geometry and composition.

In surface-based methods, only the surface of a scattering body is discretized. T-matrix method is one of the surface-based methods and requires less computer demand.

T-matrix method is one of the widely used theoretical techniques for the computation of scattering by single and composite particles, discrete random media, and particles in the vicinity of an interface separating two half-spaces with different refractive indices (Mishchenko et al. 2002).

In this study, to simulate the scattering effects from nonspherical particles, we used the T-matrix algorithm included in ScatLab1.2 software developed by Volodymyr Bazhan for light scattering investigations (WEB_5 2007). We also used the software SScaTT superellipsoid scattering tool (WEB_6 2007) to generate different ellipsoids with desired parameters consistent to our samples and analyzing their polarization effects.

4.2. T-Matrix Method

This technique also called with different names such as the null-field method and extended boundary condition method (Mishchenko et al. 2002). The T-matrix method was first developed by Waterman (1965,1971) as a technique for computing electromagnetic scattering by single, homogenous, and arbitrarily shaped particles. Each field (the incident, transmitted and scattered field) can be expanded into a series of spherical vector wavefunctions as will be shown for the scattered field.

In a three-dimensional space D consisting of a closed surface S, its interior D_i and its exterior D_s, the transmission boundary-value problem satisfy the Maxwell's equations

$$\left.\begin{aligned} \nabla \times \boldsymbol{E}_t &= jk\mu_t \boldsymbol{H}_t \\ \nabla \times \boldsymbol{H}_t &= -jk\varepsilon_t \boldsymbol{E}_t \end{aligned}\right\} \tag{4.2}$$

where $\boldsymbol{E}_t$ is denoted for the both interior and exterior electric fields $\boldsymbol{E}_i$ and $\boldsymbol{E}_s$. $\boldsymbol{H}_t$ represents the interior and exterior magnetic fields $\boldsymbol{H}_i$ and $\boldsymbol{H}_s$.

Solving this transmission boundary-value problem using the null-field method with discrete sources required the scattering object to be replaced by a set of surface current densities $\boldsymbol{e}$ and $\boldsymbol{h}$. The discrete source can be vector spherical functions, magnetic and electric dipoles or Mie potentials. The exact solution can be analyzed by the following three steps (Wriedt 2002):

(I) The null-field method with discrete sources consist in a set of integral equations (null-field equations) for the surface current densities $\boldsymbol{e}$ and $\boldsymbol{h}$. Utilizing the boundary conditions, these equations are obtained as following:

$$\left.\begin{aligned}\int_S \left[(\boldsymbol{e}-\boldsymbol{e}_0).\Psi_v^3 + j\sqrt{\frac{\mu_s}{\varepsilon_s}}(\boldsymbol{h}-\boldsymbol{h}_0).\varphi_v^3 \right] dS = 0 \\ \int_S \left[(\boldsymbol{e}-\boldsymbol{e}_0).\varphi_v^3 + j\sqrt{\frac{\mu_s}{\varepsilon_s}}(\boldsymbol{h}-\boldsymbol{h}_0).\Psi_v^3 \right] dS = 0\end{aligned}\right\} v = 1,2,3.. \tag{4.3}$$

where $\boldsymbol{e}_0 = \boldsymbol{n}\times\boldsymbol{E}_0$ and $\boldsymbol{h}_0 = \boldsymbol{n}\times\boldsymbol{H}_0$ are the tangential components of the incident electric field $\boldsymbol{E}_0$ and incident magnetic field $\boldsymbol{H}_0$. The set $\{\Psi_v^3, \varphi_v^3\}$ consists of radiating solutions to Maxwell equations $\{\Psi_v^1, \varphi_v^1\}$, and related to the used discrete source system (vector spherical functions, magnetic and electric dipoles or Mie potentials). The localized vector spherical functions $\{\boldsymbol{M}_{mn}^{1,3}, \boldsymbol{N}_{mn}^{1,3}\}_{m\in Z, n\geq \max(1,|m|)}$ are:

$$\begin{aligned}\boldsymbol{M}_{mn}^{1,3}(kx) &= \sqrt{D_{mn}}\, z_n(kr)\left[jm\frac{P_n^{|m|}\cos(\theta)}{\sin\theta}\boldsymbol{e}_\theta - \frac{dP_n^{|m|}\cos(\theta)}{d\theta}\boldsymbol{e}_\varphi \right] e^{jm\varphi}, \\ \boldsymbol{N}_{mn}^{1,3}(kx) &= \sqrt{D_{mn}}\left\{ n(n+1)\frac{z_n(kr)}{kr}P_n^{|m|}\cos(\theta)e^{jm\varphi}\boldsymbol{e}_r \right. \\ &\left. + \frac{krz_n(kr)}{kr}\left[\frac{dP_n^{|m|}\cos(\theta)}{d\theta}\boldsymbol{e}_\theta + jm\frac{P_n^{|m|}\cos(\theta)}{\sin\theta}\boldsymbol{e}_\varphi \right] \right\} e^{jm\varphi}\end{aligned} \tag{4.4}$$

where z_n represents the spherical Bessel functions j_n or the spherical Hankel functions of the first kind h_n^1, $P_n^{|m|}$ is the related Legendre polynomial of order n and m, D_{mn} is a

normalization constant dependent to the orders *n* and *m*, and $(\boldsymbol{e}_r, \boldsymbol{e}_\theta, \boldsymbol{e}_\varphi)$ are the unit vectors in spherical coordinates.

(II) Assuming the system $\{\boldsymbol{n}\times\Psi_\mu^1, \boldsymbol{n}\times\phi_\mu^1\}_{\mu=1}^{\infty}$ is a Schauder basis, there exist a sequence $\{a_\mu, b_\mu\}_{\mu=1}^{\infty}$, and then the solution of Eqs.(4.3), surface current densities $\boldsymbol{e}$ and $\boldsymbol{h}$, are can be approximated by fields of discrete sources as following:

$$\left.\begin{aligned}\boldsymbol{e}(\boldsymbol{y}) &= \sum_{\mu=1}^{\infty} a_\mu \boldsymbol{n}\times\Psi_\mu^1(k_i\boldsymbol{y}) + b_\mu \boldsymbol{n}\times\phi_\mu^1(k_i\boldsymbol{y}) \\ \boldsymbol{h}(\boldsymbol{y}) &= -j\sqrt{\frac{\varepsilon_i}{\mu_i}}\sum_{\mu=1}^{\infty} a_\mu \boldsymbol{n}\times\phi_\mu^1(k_i\boldsymbol{y}) + b_\mu \boldsymbol{n}\times\Psi_\mu^1(k_i\boldsymbol{y})\end{aligned}\right\} \boldsymbol{y}\in S \tag{4.5}$$

(III) The scattered field is obtained by using the representation theorem. The series expansion of the scattered field into radiating spherical vector wave functions given as

$$\boldsymbol{E}_s(\boldsymbol{x}) = \sum_{v=1}^{\infty} f_v \boldsymbol{M}_v^3(k_s\boldsymbol{x}) + g_v \boldsymbol{N}_v^3(k_s\boldsymbol{x}) \tag{4.6}$$

where

$$\begin{aligned} f_v &= \frac{jk_s^2}{\pi}\int_S \left[\boldsymbol{e}(\boldsymbol{y}).\boldsymbol{N}_{\bar{v}}^1(k_s\boldsymbol{y}) + j\boldsymbol{h}(\boldsymbol{y}).\boldsymbol{M}_{\bar{v}}^1(k_s\boldsymbol{y})\right] dS(\boldsymbol{y}) \\ g_v &= \frac{jk_s^2}{\pi}\int_S \left[\boldsymbol{e}(\boldsymbol{y}).\boldsymbol{M}_{\bar{v}}^1(k_s\boldsymbol{y}) + j\boldsymbol{h}(\boldsymbol{y}).\boldsymbol{N}_{\bar{v}}^1(k_s\boldsymbol{y})\right] dS(\boldsymbol{y}) \end{aligned} \tag{4.7}$$

In these equations $\bar{v}$ is a complex index included both –*m* and *n*; $\bar{v} = (-m, n)$.

In order to drive the T-matrix, the incident field inside a finite region containing *S* can be also expressed as a series of regular vector spherical functions with analogy to the (4.6):

$$\left.\begin{aligned} \boldsymbol{E}_0(\boldsymbol{x}) &= \sum_{v=1}^{\infty} a_v^0 \boldsymbol{M}_v^1(k_s\boldsymbol{x}) + b_v^0 \boldsymbol{N}_v^1(k_s\boldsymbol{x}) \\ \boldsymbol{H}_0(\boldsymbol{x}) &= -j\sqrt{\frac{\varepsilon_s}{\mu_s}} \sum_{v=1}^{\infty} a_v^0 \boldsymbol{N}_v^1(k_s\boldsymbol{x}) + b_v^0 \boldsymbol{M}_v^1(k_s\boldsymbol{x}) \end{aligned}\right\} \tag{4.8}$$

The linear relation between the scattered and the incident field coefficients in Eqs. (4.3) and (4.8), obtained as

$$\begin{bmatrix} f_v \\ g_v \end{bmatrix} = \boldsymbol{T} \begin{bmatrix} a_v^0 \\ b_v^0 \end{bmatrix} \tag{4.9}$$

where $\boldsymbol{T}$ is the transition matrix (T-matrix) given as

$$\boldsymbol{T} = \boldsymbol{B}\boldsymbol{A}^{-1}\boldsymbol{A}_0 . \tag{4.10}$$

$\boldsymbol{A}$, $\boldsymbol{B}$, and $\boldsymbol{A_0}$ are are block matrices written in general,

$$\boldsymbol{X} = \begin{bmatrix} X_{v\mu}^{11} & X_{v\mu}^{11} \\ X_{v\mu}^{11} & X_{v\mu}^{11} \end{bmatrix}, v, \mu = 1,\ 2,..., \tag{4.11}$$

where $\boldsymbol{X}$ standing for $\boldsymbol{A}$, $\boldsymbol{B}$ and $\boldsymbol{A}_0$. The expressions for the elements of these matrices are given in the Appendix.

While the exact infinite T-matrix is independent of the expansion systems used on *S*, there exists such dependence for the truncated matrix

$$\boldsymbol{T}_N = \boldsymbol{B}_N \boldsymbol{A}_N^{-1} \boldsymbol{A}_{0N} \tag{4.12}$$

computed according to the far field approximation and called approximate truncated matrix.

T-matrix depends on the incident wavelength and particle shape, its refractive index and its relation to the coordinate system. To perform scattering computations, the T-matrix method is considered of having advantage to the other methods because of the all polarization information depended to the scattering effects is included in the T-

matrix. Thus by computing the T-matrix in a scattering problem under slightly different conditions of incident light wave, the orientation or scattering angles can be computed. In addition, the orientation-averaged scattering quantities can be obtained with different ways using T-matrix (Wriedt 2002).

A detailed theoretical explanation can be found in the book by Mishchenko et al (Mishchenko et al 2002). Mishchenko has developed several public domain programs which are available at the internet.

4.3. Normalized Differential Scattering Cross-Section (DSCS)

The normalized differential scattering cross-section (DSCS), is widely used for characterization of the scattering intensity computed from the far-field pattern such as the efficiency factor Q_{sca} given in the previous chapter.

DSCS depends on the polarization state of the incident light as well as on the incidence and scattering directions. The angle-dependent scattering intensity functions for *p* and *s*-polarized components of the far-field pattern plotted in Fig.4.1. is DSCS,

$$\frac{dC_{sca}}{d\Omega} = \frac{\left|k_s \boldsymbol{E}_{s0}^{N}\right|^2}{\pi \left|k_s a\right|^2} \tag{4.13}$$

where $\boldsymbol{E}_{s0}^{N}$ is the far field pattern of the unit incident electric field and a is a characteristic dimension of the particle.

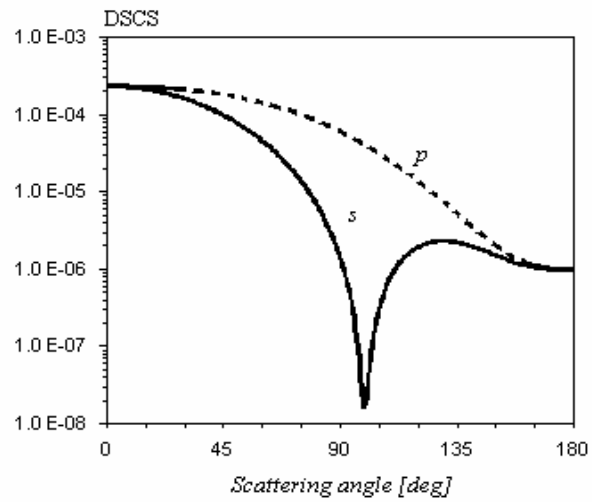

Figure 4.1. Differential scattering cross-section of spheroid a=b=2400nm, c=4800nm, m=1.453, $\lambda = 632{,}8$ nm.

4.4. Simulation Results

The software SScaTT superellipsoid scattering tool used to generate different ellipsoids, especially spheroid models consistent to polymeric particles deposited to optical thin films used in LCD backlight systems. These types of particles are nonabsorbing (dielectric) and have large size compared to the wavelength.

The simulation results are summarized for oblate and prolate spheroids with difference size and aspect ratios. The simulations for spherical particles are also included in order to represent the difference between polarization effects of nonspherical and spherical scatterers.

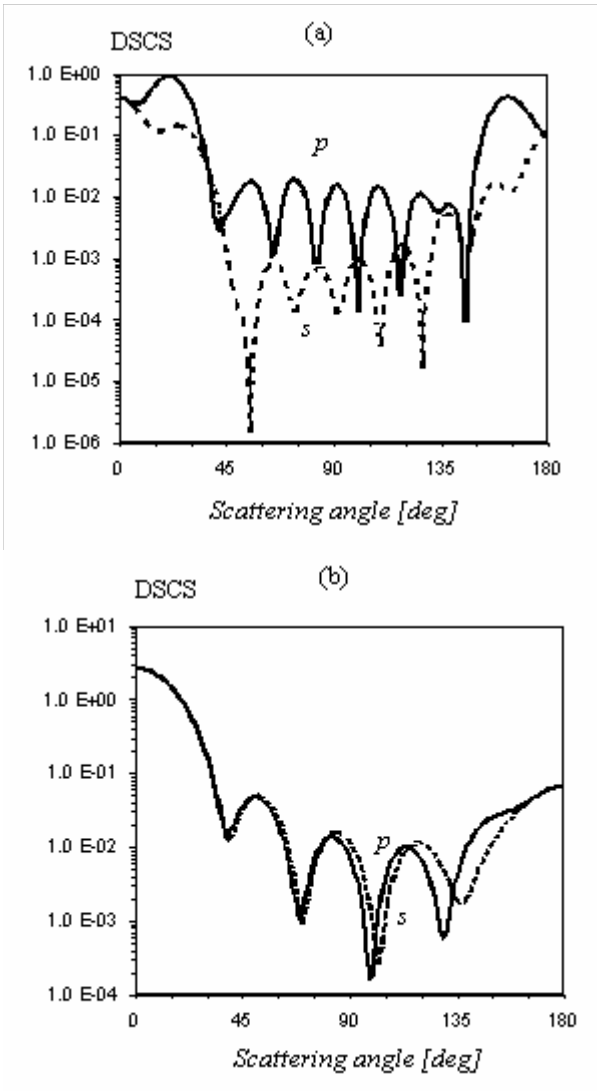

105372 faces,52688 vertices (prolate spheroid)

a=1.000000;
b=1.000000;
c=4.000000;
e=1.000000;
n=1.000000;
delta=0.053500;
eps=0.110000;
wavelength=0.632800;
refractive_idx_re=1.4539;
refractive_idx_im=0.000000;
normalization radius=1.000;
Nrank=10;
Mrank=10;

33060 faces,16532 vertices (sphere)

a=1.000000;
b=1.000000;
c=1.000000;
e=1.000000;
n=1.000000;
delta=0.053500;
eps=0.110000;
wavelength=0.632800;
refractive_idx_re=1.4539;
refractive_idx_im=0.000000;
normalization radius=1.000;
Nrank=5;
Mrank=3;

Figure 4.2. (a) Differential scattering cross-section of prolate spheroid a= b=1μm, c=4 μm, and (b) Differential scattering cross-section of sphere a= b= c=1μm and the normalization radius r(norm)=1 μm (m=1.453, λ = 632,8 nm)

The incident light in all of these simulations was taken as linearly 45^0 polarized. In order to obtain the relation of polarization effects to the scatterer geometry, the refractive index, wavelength and polarization state of incidence light were kept constant overall of the simulations.

Fig.4.2(a) is the simulation result for a dielectric prolate spheroid with refractive index m=1.45 and with aspect ratio c/a=4 and Fig.4.2(b) is the simulation result for the spherical particle of the same material with $a = b = c = 1\mu m$. The differential scattering cross-section (DSCS) of prolate spheroid indicated an intensity gain in p-polarized component relative to the s- polarized component for almost all scattering regions including the interested small scattering angles $\theta < 30^0$ in forward direction. On the other hand the DSCS of spherical particle in Fig.4.2(b) represented polarization discrimination only for some backscattering regions. From these results, the impossibility of polarization enhancement by forward scattering may be concluded for usage of spherical geometries.

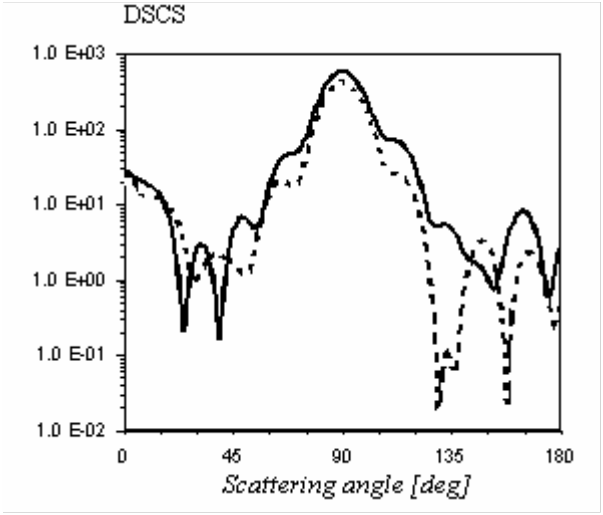

291112 faces, 145558 vertices (oblate spheroid)

a=4.000000;
b=4.000000;
c=1.000000;
e=1.000000;
n=1.000000;
delta=0.05350;
eps=0.110000;
wavelength=0.632800;
refractive_idx_re=1.4539;
refractive_idx_im=0.000000;
normalization radius=1.000;
Nrank=10;
Mrank=10;

Figure 4.3. Differential scattering cross-section of oblate spheroid a= b=4μm, c=1μm and r(norm)=1 μm (m=1.453, $\lambda = 632{,}8$ nm)

Fig.4.3 is the simulation result for a dielectric oblate spheroid with refractive index m=1.45 and with aspect ratio c/a=0.25. The DSCS of oblate spheroid indicated less significant polarization discrimination compared to the of prolate one given in Fig.4.2(a) for the interested small scattering angles $\theta < 30^0$.

Fig.4.5 and Fig.4.6 are the simulation results for a dielectric prolate spheroid with refractive index m=1.45 and with aspect ratio c/a=3.75. The figures of DSCS represented more significant polarization discrimination in favour of s-polarization compared to of prolate one given in Fig.4.2(a) especially at the forward scattering angles (see Fig.4.4). The shift between two results caused from the difference in normalization radius defined by (4.13).

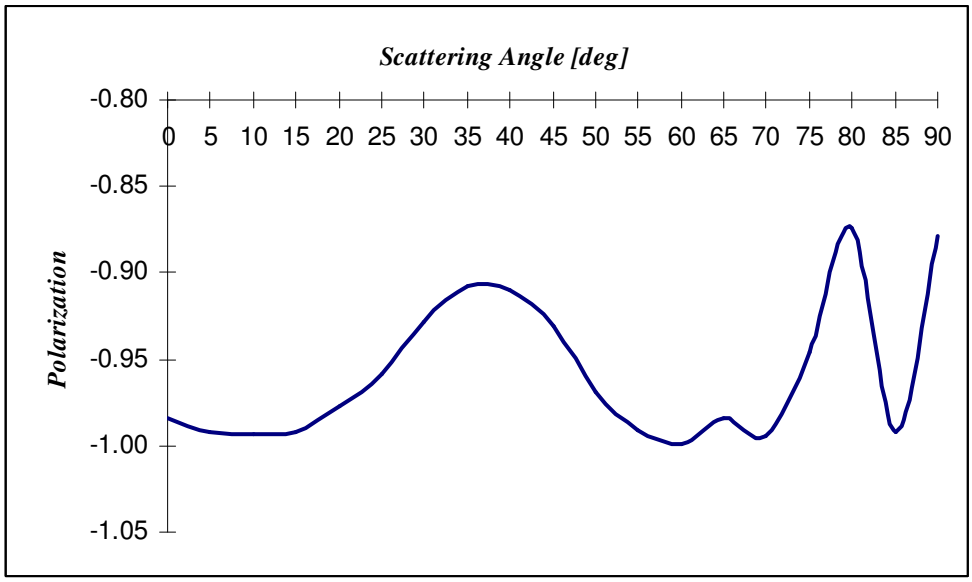

Figure 4.4. Polarization of scattered light by prolate spheroid a= b=0.8μm, c=3 μm and r(norm)=0.8 μm (m=1.453, $\lambda = 632{,}8$ nm)

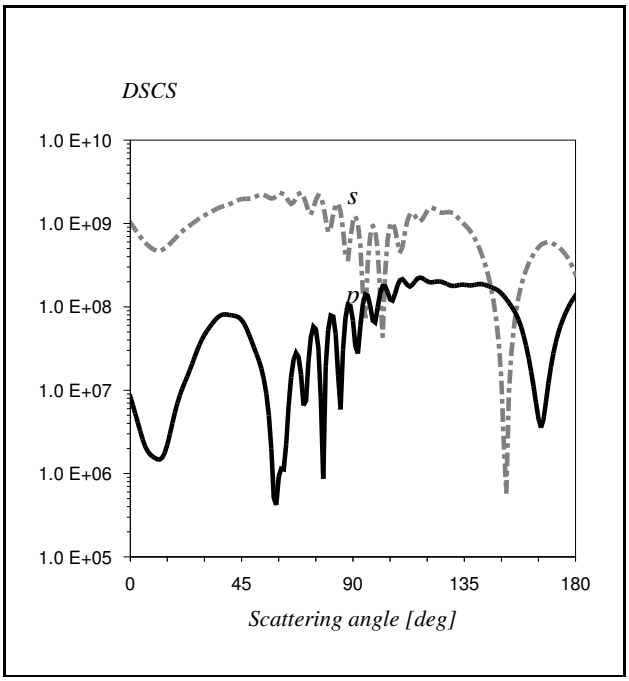

684 faces,344 vertices
(prolate spheroid)

a=0.800000;
b=0.800000;
c=3;
e=1.000000;
n=1.000000;
delta=0.5;
wavelength=0.632800;
refractive_idx_re=1.4539;
refractive_idx_im=0.000000;
normalization radius=0.800;
Nrank=32;
Mrank=22;

Figure 4.5. Differential scattering cross-section of prolate spheroid a= b=0.8μm, c=3 μm and r(norm)=0.8 μm (m=1.453, $\lambda = 632{,}8$ nm)

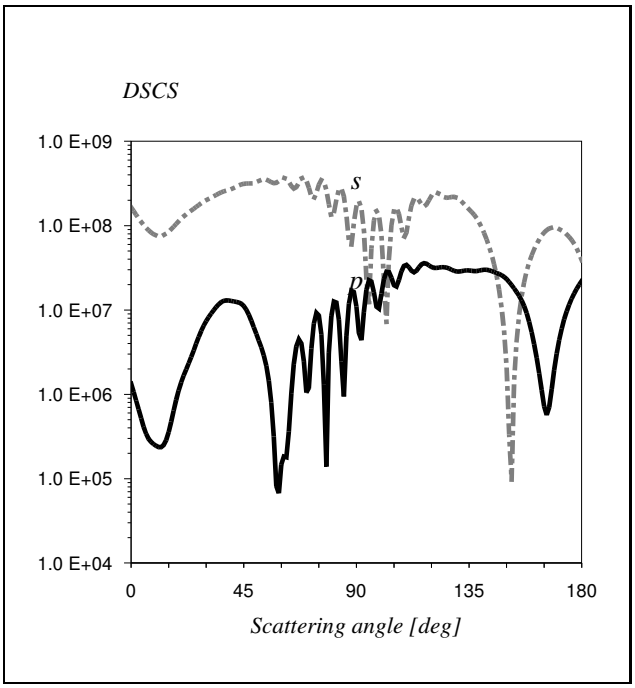

684 faces,344 vertices
(prolate spheroid)

a=0.800000;
b=0.800000;
c=3;
e=1.000000;
n=1.000000;
delta=0.5;
wavelength=0.632800;
refractive_idx_re=1.4539;
refractive_idx_im=0.000000;
radius_norm=2.000000;
Nrank=32;
Mrank=22;

Figure 4.6. Differential scattering cross-section of prolate spheroid *a*= *b*=0.8μm, c=3 μm and r(norm)=2 μm (m=1.453, $\lambda = 632{,}8$ nm)

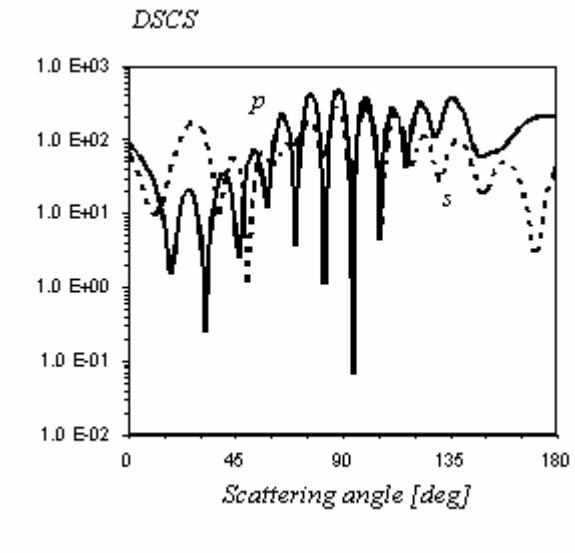

476 faces,240 vertices
(prolate spheroid)

a=0.800000;
b=0.800000;
c=1.800000;
e=1.000000;
n=1.000000;
delta=0.5;
eps=0.110000;
wavelength=0.632800;
refractive_idx_re=1.4539;
refractive_idx_im=0.000000;
radius_norm=0.800000;
Nrank=20;
Mrank=12;

Figure 4.7. Differential scattering cross-section of prolate spheroid *a*= *b*=0.8μm, c=1.8 μm and r(norm)=0.8 μm (m=1.453, $\lambda = 632{,}8$ nm)

Fig.4.7 is the simulation result for a dielectric prolate spheroid with refractive index *m*=1.45 and with aspect ratio *c/a*=2.25. The DSCS of this spheroid indicated a gain in favour of *p*-polarized component for scattering angles $0 < \theta < 10^0$, and in favour of *s*-polarized component at scattering angles $10^0 < \theta < 45^0$ in forward direction.

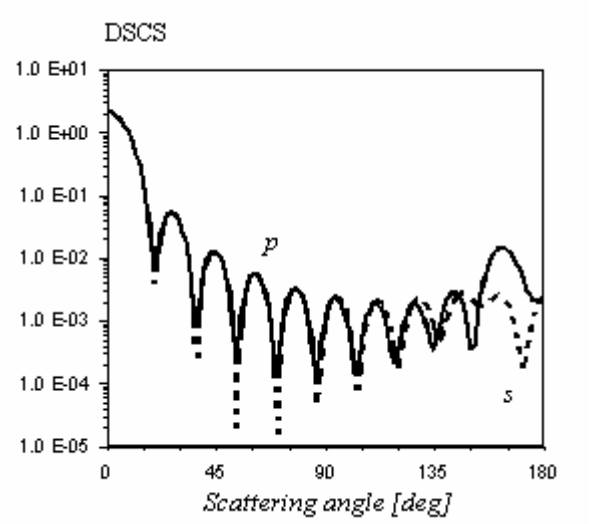

6420 faces, 3212 vertices(sphere)

a=4.000000;
b=4.000000;
c=4.000000;
e=1.000000;
n=1.000000;
delta=0.50;
eps=0.110000;
wavelength=0.632800;
refractive_idx_re=1.4539;
refractive_idx_im=0.000000;
radius_norm=4.000000;
Nrank=10;
Mrank=10;

Figure 4.8. Differential scattering cross-section of sphere a= b= c=4μm and r(norm)=4μm (m=1.453, $\lambda = 632{,}8$ nm)

The DSCS of spherical particle in Fig.4.8 represented polarization discrimination only for some backscattering regions similar to results given in Fig.4.2(b).

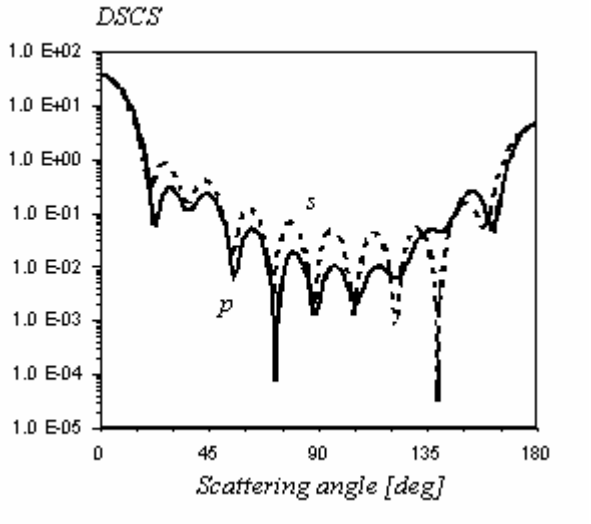

80176 faces, 4090 vertices (prolate spheroid)

a=1.000000;
b=1.000000;
c=3.000000;
e=1.000000;
n=1.000000;
delta=0.05350;
eps=0.110000;
wavelength=0.632800;
refractive_idx_re=1.4539;
refractive_idx_im=0.000000;
radius_norm=1.000000;
Nrank=10;
Mrank=10;

Figure 4.9. Differential scattering cross-section of prolate spheroid a= b=1μm, c=3μm and r(norm)=1μm (m=1.453, $\lambda = 632{,}8$ nm)

Fig.4.9 is the simulation result for a dielectric prolate spheroid with refractive index m=1.45 and with aspect ratio c/a=3. The DSCS of this spheroid indicated an intensity gain in favour of s-polarized component at scattering angles around the region $20^0 < \theta < 45^0$.

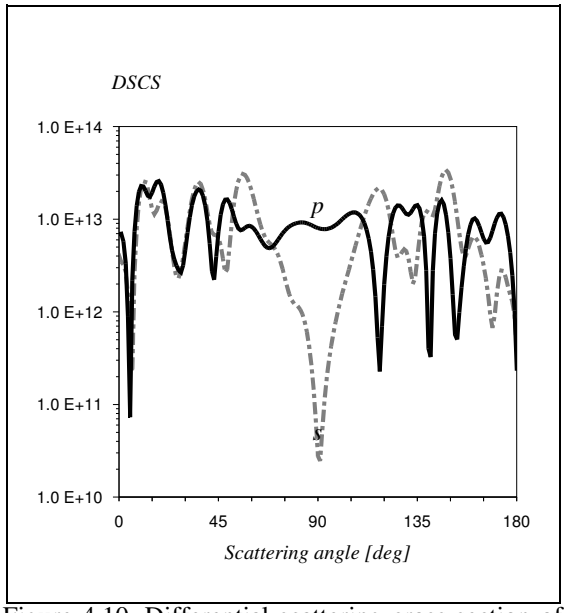

1868 faces, 936 vertices
(oblate spheroid)

a=3.000000;
b=3.000000;
c=1.000000;
e=1.000000;
n=1.000000;
delta=0.5;
eps=0.11;
wavelength=0.632800;
refractive_idx_re=1.4539;
refractive_idx_im=0.000000;
radius_norm=2.000000;
Nrank=32;
Mrank=22;

Figure 4.10. Differential scattering cross-section of oblate spheroid *a*= *b*=3μm, c=1μm and r(norm)=2μm (m=1.453, $\lambda = 632{,}8$ nm)

Fig.4.10 is the simulation result for a dielectric oblate spheroid with refractive index *m*=1.45 and with aspect ratio *c/a*=0.33. The DSCS of this oblate spheroid indicated polarization discrimination in forward direction only for a small region around $15^0 < \theta < 20^0$ (see Fig.4.11).

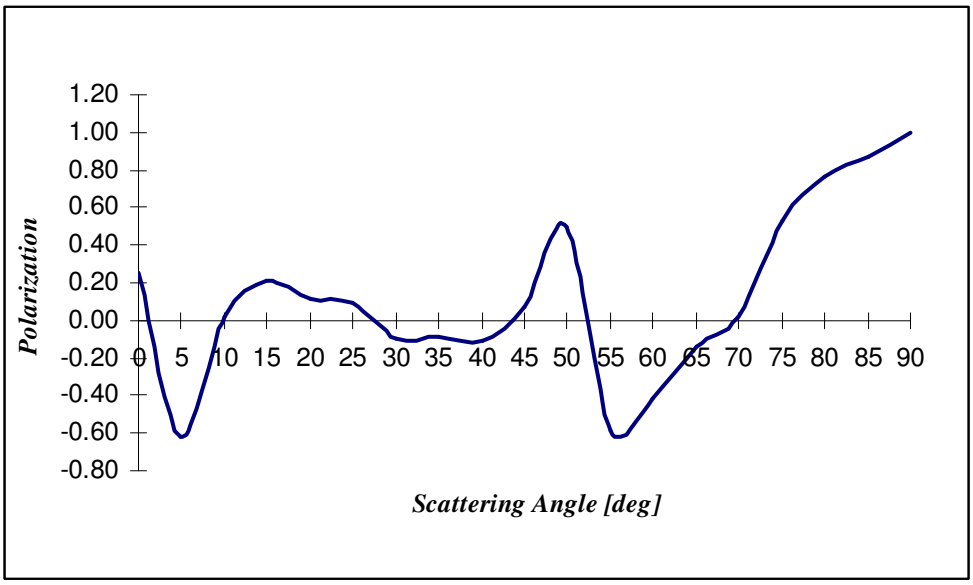

Figure 4.11. Polarization of scattered light by oblate spheroid *a*= *b*=3μm, c=1μm and r(norm)=2μm (m=1.453, $\lambda = 632{,}8$ nm)

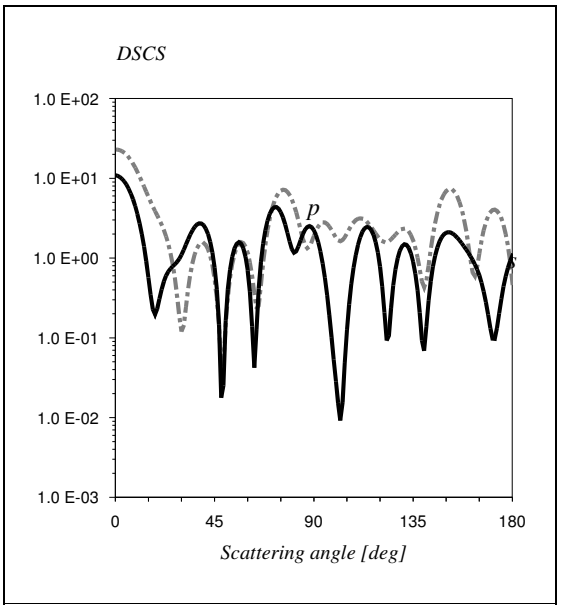

360 faces, 182
vertices(prolate spheroid)

a=1.000000;
b=1.000000;
c=1.200000;
e=1.000000;
n=1.000000;
delta=0.5;
eps=0.11;
wavelength=0.632800;
refractive_idx_re=1.4539;
refractive_idx_im=0.000000;
radius_norm=1.000000;
Nrank=20;
Mrank=12;

Figure 4.12. Differential scattering cross-section of prolate spheroid *a*= *b*=1μm, c=1.2μm and r(norm)=1μm (m=1.453, $\lambda = 632{,}8$ nm)

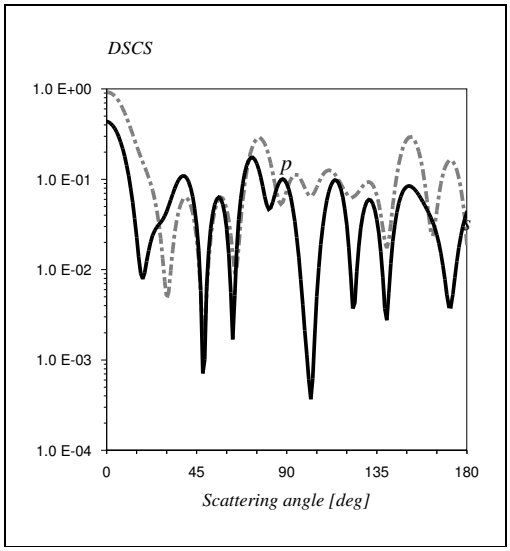

360 faces, 182
vertices(prolate spheroid)

a=1.000000;
b=1.000000;
c=1.200000;
e=1.000000;
n=1.000000;
delta=0.5;
eps=0.11;
wavelength=0.632800;
refractive_idx_re=1.4539;
refractive_idx_im=0.000000;
radius_norm=5.000000;
Nrank=20;
Mrank=12;

Figure 4.13. Differential scattering cross-section of prolate spheroid *a*= *b*=1μm, c=1.2μm and r(norm)=5μm (m=1.453, $\lambda = 632{,}8$ nm)

Fig.4.12 and Fig.4.13 are the simulation results for a dielectric prolate spheroid with refractive index *m*=1.45 and with aspect ratio *c/a*=1.2. The figures of DSCS represented polarization discriminations in favor of *s*-polarization for scattering angles $0^0 < \theta < 26^0$ and in favor of *p*-polarization at scattering angles $26^0 < \theta < 56^0$ (see Fig.4.14) in forward direction.

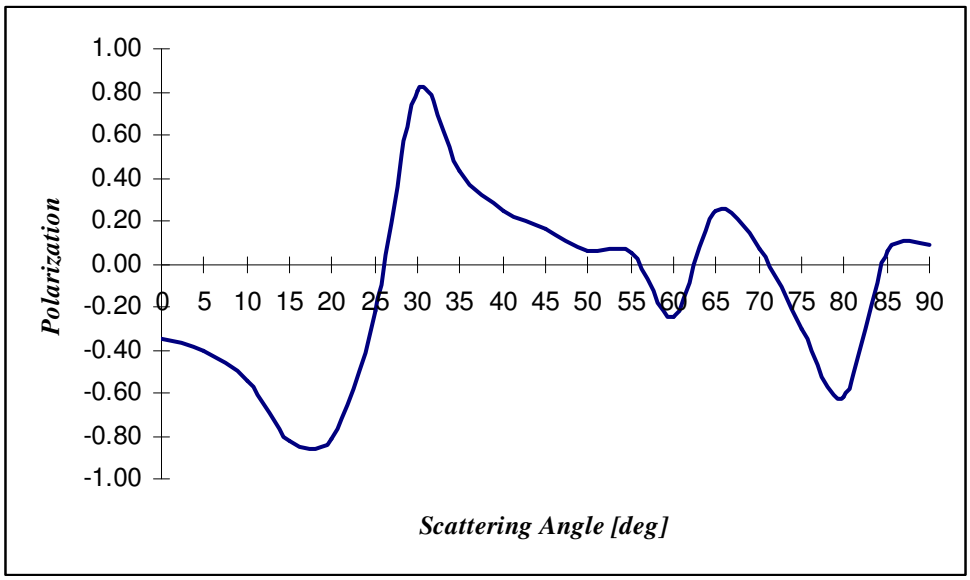

Figure 4.14. Polarization of scattered light by prolate spheroid *a*= *b*=1μm, c=1.2μm and r(norm)=5μm (m=1.453, $\lambda = 632{,}8$ nm)

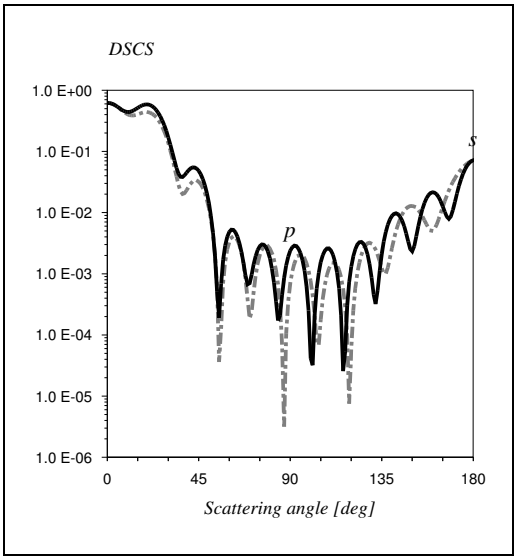

1992 faces, 998 vertices
(prolate spheroid)

a=2.000000;
b=2.000000;
c=3;
e=1.000000;
n=1.000000;
delta=0.5;
eps=0.11;
wavelength=0.632800;
refractive_idx_re=1.4539;
refractive_idx_im=0.000000;
radius_norm=1.500000;
Nrank=10;
Mrank=10;

Figure 4.15. Differential scattering cross-section of prolate spheroid *a*= *b*=2μm, c=3μm and r(norm)=5μm (m=1.453, $\lambda = 632{,}8$ nm)

Fig.4.15 and Fig.4.16 are the simulation results for a dielectric prolate spheroid with refractive index *m*=1.45 and with aspect ratio *c/a*=1.5. The DSCS of this spheroid indicated an intensity gain in favor of *p*-polarized component at scattering angles around the region $10^0 < \theta < 20^0$ in forward direction.

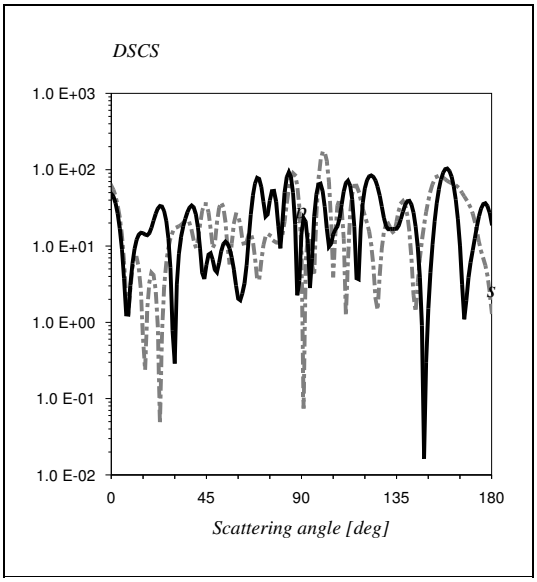

1992 faces, 998 vertices
(prolate spheroid)

a=2.000000;
b=2.000000;
c=3;
e=1.000000;
n=1.000000;
delta=0.5;
eps=0.11;
wavelength=0.632800;
refractive_idx_re=1.4539;
refractive_idx_im=0.000000;
radius_norm=1.500000;
Nrank=32;
Mrank=22;

Figure 4.16. Differential scattering cross-section of prolate spheroid *a*= *b*=2μm, c=3μm and r(norm)=1.5μm (m=1.453, $\lambda = 632{,}8$ nm)

CHAPTER 5

POLARIZATION MEASUREMENTS

A number of methods exist in order to measure the parameters and polarization characteristics of dielectric filters. In the manufacturing of microelectronic and microoptic elements, the measurement coefficients of material refraction and absorption as well as the layer homogeneity and thickness is an important task (Kalimanova et al. 2005). The most common optical measurement technique is ellipsometry. Ellipsometry is an extremely sensitive used to characterize thin films by observing the relative phase change in a polarized light beam reflected from the film surface.

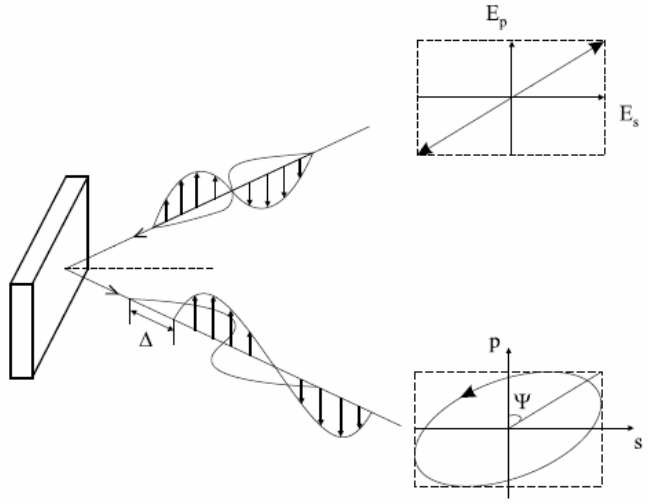

Figure 5.1. Schematic drawing of ellipsometry

However, the accuracy of this type of measurement suffers from scattering losses. In addition, reflection and transmission measurements are not sensitive to small phase shifts. Normal ellipsometry measurements are usually not capable of measuring characteristics of very complicated samples that may contain depolarization or cross-polarization (Jellison 2004).

5.1. Ellipsometry Measurements

When linearly polarized light is reflected or transmitted from a surface, a phase shift in the both components take place. Since this shift is in general not the same for both components, resulting light is in an elliptically polarized state. The name ellipsometry is used for the technique of measuring this change in polarization of light.

The parameters such as refractive index, extinction coefficient and thickness of the material are obtainable by correct analysis of the results obtained from the ellipsometric measurements. Two most common methods of determining these parameters of thin film are single ellipsometric measurements used in our study and multiple wavelengths spectroscopic ellipsometry.

Accessing to full Mueller matrix parameters allows us to have a complete picture of the material for the correct characterization. Mueller matrix describes perfectly the polarization change due to a sample. Examples of the benefits gained by the Mueller matrix formalism are found when characterizing gratings and anisotropic samples.

The basic interest for ellipsometry is the measurement of polarization changes in the *p*- and *s*-components upon reflection or transmission relative to each other. A known polarization is reflected or transmitted from the sample and the output polarization is measured.

5.2. The Fundamental Equation of Ellipsometry

Ellipsometry measures two values, Ψ and Δ. Ψ is the angle whose tangent is the ratio of the magnitudes of the reflection (or transmission) coefficients and Δ is the change in phase. By using these measured values, the fundamental equations of ellipsometry is given as following for the cases reflection and transmission respectively:

$$\left.\begin{aligned} \rho_r &= \frac{r_p}{r_s} = \tan\Psi_r \exp(j\Delta_r) \\ \rho_t &= \frac{t_p}{t_s} = \tan\Psi_t \exp(j\Delta_t) \end{aligned}\right\}. \qquad (5.1)$$

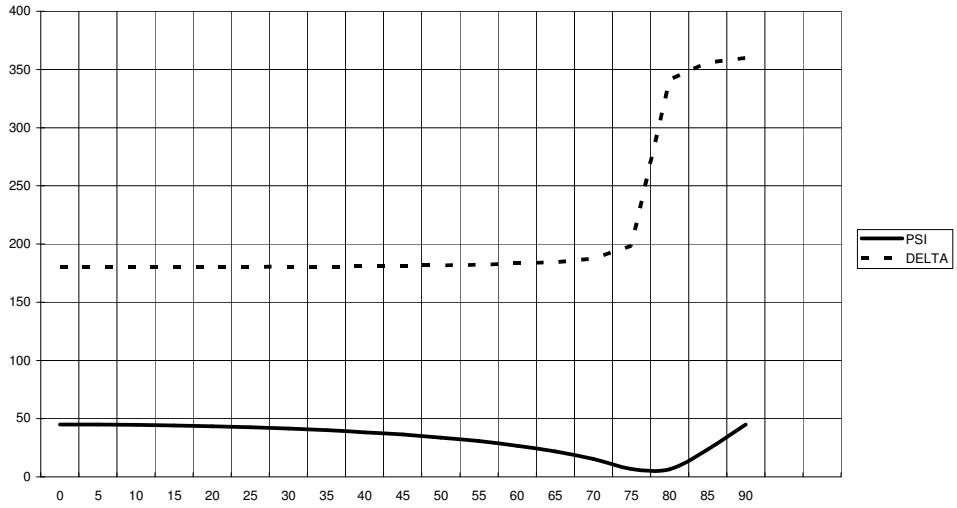

Figure 5.2. The variation of Ψ and Δ with incident angle

Ψ vary between 0 and $\pi/2$ and Δ vary between 0 and 2π. These values are related to the Fresnel reflection coefficients r_p and r_s, in the reflection case and vice versa. All Fresnel reflection and transmission coefficients are easily can be derived from Fresnel formulas as described in Section 2.5.2.

By using this polarization ratio ρ, the real part of the refractive index n_2 and the imaginary part (the extinction coefficient) k, can be obtained. In addition, these obtained values used to calculate the absorption coefficient,

$$\alpha = \frac{4\pi k}{\lambda} \tag{5.2}$$

5.3. Spectroscopic Ellipsometry

Spectroscopic measurements require a method of wavelength selection. By changing the wavelength of light, (Ψ, Δ) spectra and ρ are measured for transmission or reflection, as a function of wavelength (Fujiwara 2007).

Each wavelength will introduce a new unknown refractive index. Spectroscopic phase modulated ellipsometers (SPME) use photoelastic devices to perform the polarization modulation at each wavelength. This offers the advantage of modulation three orders of magnitude faster than the mechanical rotation of the polarizer. The photoelastic modulator is typically a time dependent retarder which is able to operate at very high rates of up to 50 kHz. Theoretically, very high data acquisition rates (of up to

10ms per point) can be obtained. This value is however limited by satisfactory signal-to-noise ratio levels, which require longer integration times or a very high intensity light source.

In general, the spectroscopic ellipsometry measurement is carried out in the visible region, but measurement in the infrared region has also been performed widely.

5.4. Single Wavelength Ellipsometry

Single wavelength ellipsometry uses a single frequency of light to probe the analyzed film. The optical design is simple, low-cost, and accurate. Lasers are ideal light sources with well-known wavelength and significant intensity. Single wavelength ellipsometry is more suitable for quick measurement of nominally known films. Since multiple solutions might be occurred for different film thickness, the interpretation of unknown films should be done carefully.

The refracted light may travel through different thicknesses to emerge in-phase with the first reflection, but the returning light is delayed.

The arrangement of the optical components between the source and detector defines the type of the specific ellipsometer. General two types of single wavelength ellipsometers are rotating analyzer ellipsometers and null ellipsometers. There are also different configurations where the polarizer (P), system (S), compensator (C) and analyzer (A) are may be arranged differently with respect to each other. According to such configurations, the PCSA and PSCA ellipsometer arrangements can be taken into account.

In a nulling ellipsometer, the orientation of the polarizer, compensator (or a quarter wave plate) and analyzer are adjusted with respect to each other until the light incident on the detector is nulled or extinguished. If the signal can be nulled with the analyzer, the relative phase shift between the reflected or transmitted components has been cancelled.

An example for the basic configuration of the null ellipsometer is shown in Fig.5.4. Unpolarized light passes first through a polarizer with its transmission axis.

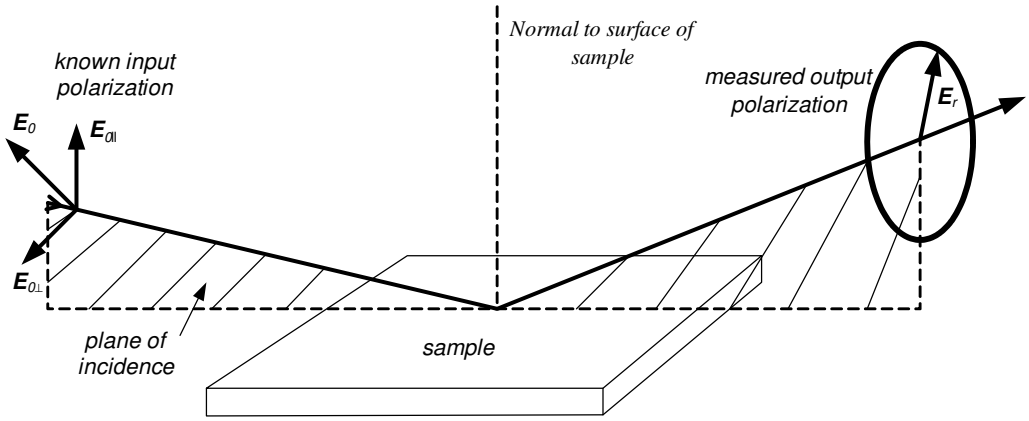

Figure 5.3. When linearly-polarized light is reflected from a material, it generally becomes elliptically polarized.

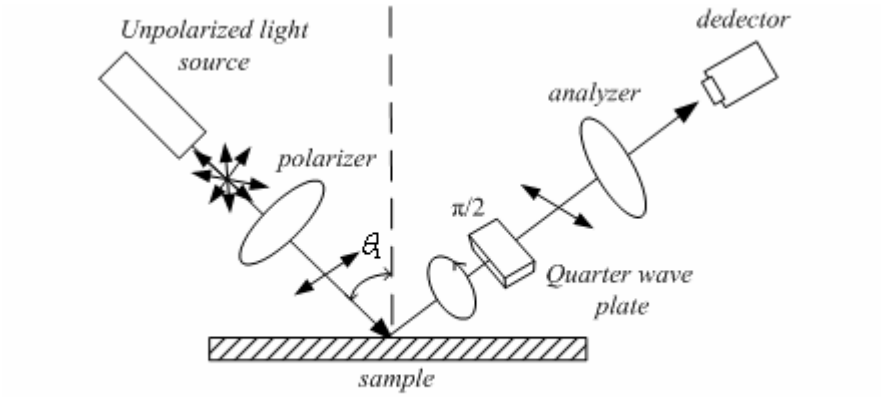

Figure 5.4. An example of null ellipsometer

Next the light reflected from the surface has elliptical state of polarization and encounters a quarter-wave plate. The wave plate introduces a $\pi/2$ phase difference between the field components, and the polarization of the emergent light is linearly polarized. The light transmitted from the wave plate passes through a second polarizer (the analyzer).

The orientations of the quarter-wave plate and the analyzer are varied until no light passes through the analyzer. Now, the light incident on the analyzer must be linearly polarized with its electric vector at angle $\pi/2$ to the analyzer's transmission axis. So, from these orientations and the direction of polarization of the incident light, the relative phase change and the relative amplitude change introduced by reflection from the surface can be calculated (WEB_3 2007, WEB_4 2007).

5.5. Experimental Results

In order to obtain the polarization characteristics of the dielectric optical film in forward direction, we used an example of the single wavelength ellipsometry as shown in Fig.5.5.

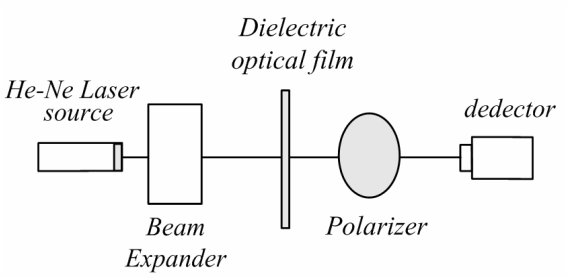

Figure 5.5. The experimental setup used in this study

The intensity measurements of scattered light performed on dielectric optical films of specific two groups used in LCD technology and on model films with and without nonspherical zeolites particles for forward scattering (scattering angle θ=0) using two laser sources with wavelengths $\lambda = 633nm$ and $\lambda = 542nm$.

First measurements performed on two optical films deposited with nonspherical random shape zeolites (see Figures 5.9), and pure film without zeolites. Measurements performed in two positions (named horizontal and perpendicular) of the film to estimate the effects of particles orientation on scattering and polarization. The measurements results and polarization states are given following.

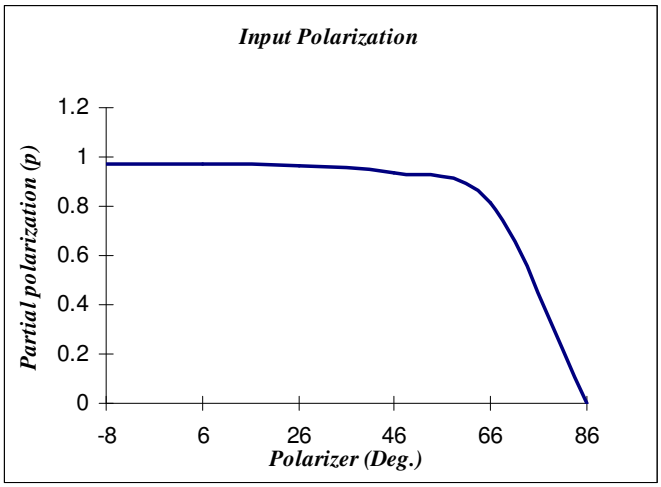

Figure 5.6. The polarization state of source (λ=633nm)

Table 5.1. Forward scattering measurements ($\theta=0^0$) and partial polarization of the output [λ=633nm, $p_0=0.97(-8^0/86^0)$]

Optical Film	polarizer (Deg)	Intensity	$p=\frac{I-I_{\min}}{I+I_{\min}}$
with zeolites (perpendicular positioned)	**-8**	**475**	**0.946721311**
	1	450	0.943844492
	21	345	0.927374302
	41	189	0.871287129
	61	59	0.638888889
	81	**13**	**0**
	86	20	0.212121212
			P_{out} =0.94 (-8/81)
with zeolites (horizontal positioned)	-8	443	0.893162393
	1	473	0.899598394
	8	**486**	**0.902152642**
	21	477	0.900398406
	41	366	0.872122762
	61	213	0.789915966
	81	78	0.514563107
	86	54	0.367088608
	101	**25**	**0**
			P_{out} =0.90 (8/101)
without zeolites	-8	**103**	**0.460992908**
	6	98	0.441176471
	26	80	0.355932203
	46	57	0.2
	66	40	0.025641026
	86	**38**	**0**
			P_{out} =0.46 (-8/86)

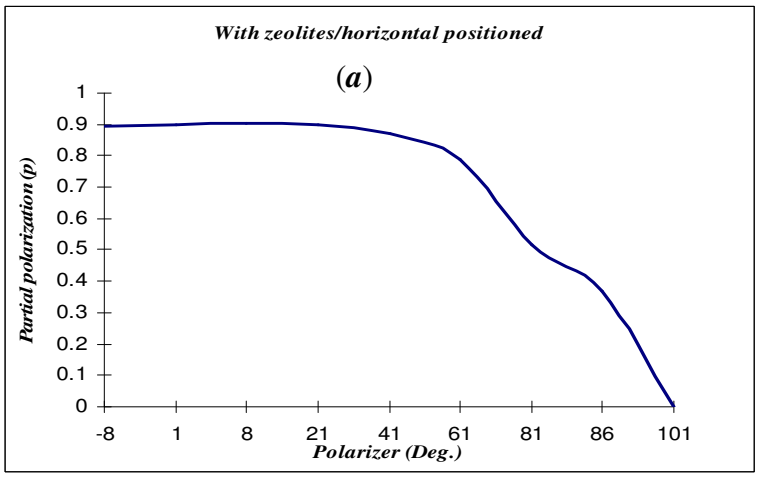

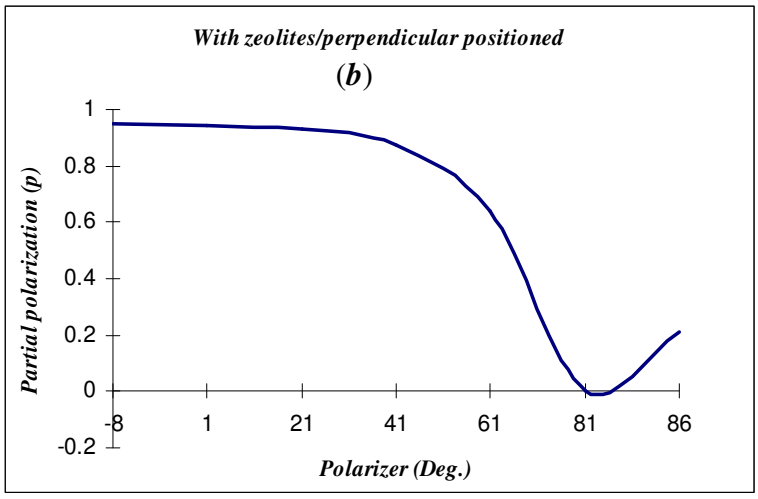

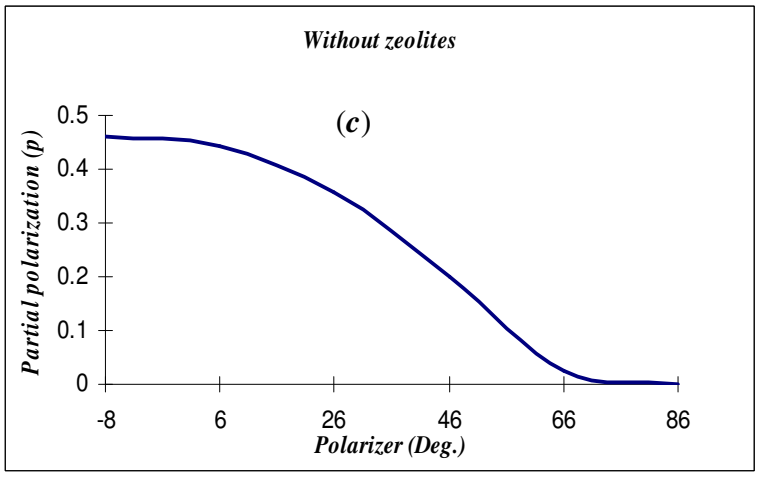

Figure 5.7. The partial polarizations of scattered light by optical film. (a) with zeolites and horizontal positioned (b) with zeolites and perpendicular positioned (c) without zeolites (λ=633nm, input polarization $p_0=0.97(-8^0-86^0)$)

Table 5.2. Forward scattering measurements ($\theta=0^0$) and partial polarization of the output [λ=542nm, $p_0=0.97(167^0/73^0)$]

Optical Film	polarizer (Deg)	Intensity	$p=\frac{I-I_{\min}}{I+I_{\min}}$
with zeolites (perpendicular positioned)	73	27	0.227272727
	93	**17**	**0**
	113	25	0.19047619
	133	49	0.484848485
	153	73	0.622222222
	167	86	0.669902913
	173	91	0.685185185
	192	**92**	**0.688073394**
			P_{out} =0.68 (93/192)
with zeolites (horizontal positioned)	73	7	0.272727273
	79	**4**	**0**
	87	8	0.333333333
	107	29	0.757575758
	127	64	0.882352941
	147	99	0.922330097
	165	113	0.931623932
	167	**115**	**0.932773109**
			P_{out} =0.93 (167/79)
without zeolites	**73**	**15**	**0**
	87	17	0.0625
	107	21	0.166666667
	127	27	0.285714286
	147	31	0.347826087
	167	**35**	**0.4**
			P_{out} =0.4 (73/167)

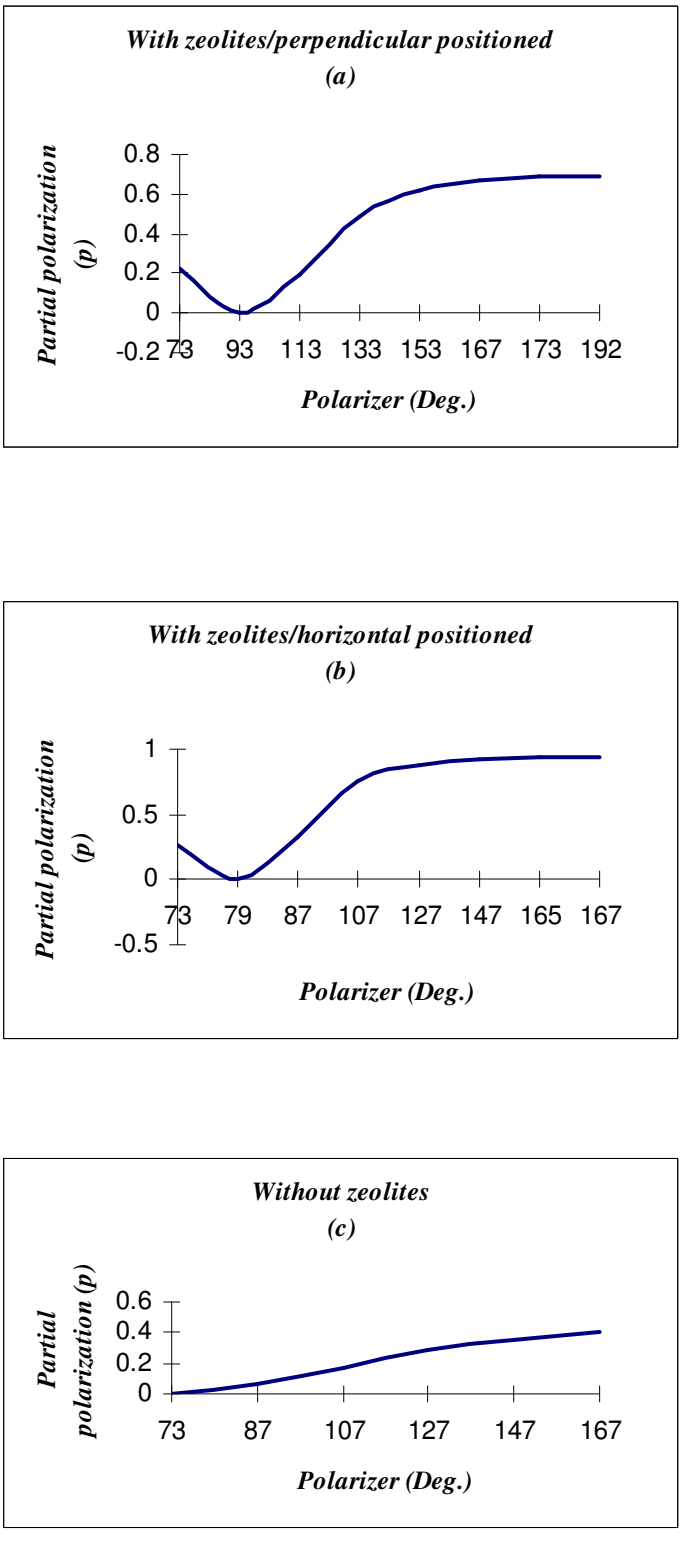

Figure 5.8. The partial polarizations of scattered light by optical film. (a) with zeolites and perpendicular positioned (b) with zeolites and horizontal positioned (c) without zeolites (λ=542nm, input polarization $p_0=1(167^0-73^0))$

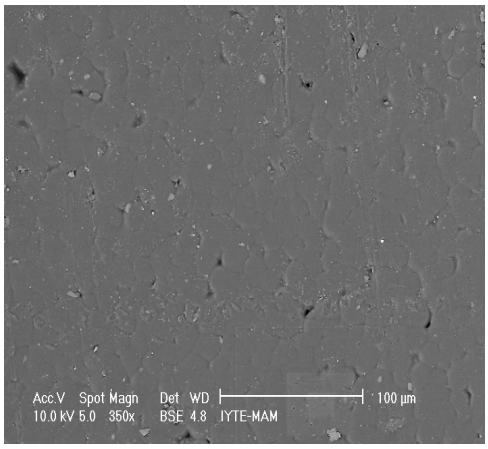

(*a*)

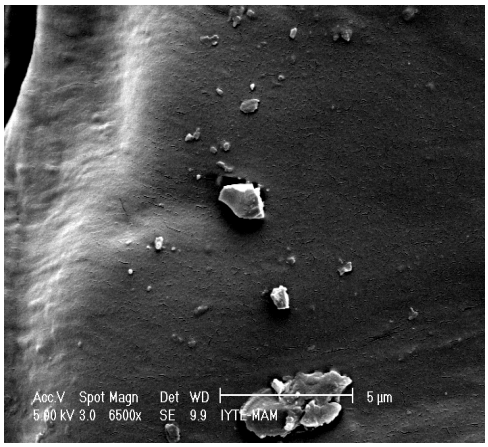

(*b*)

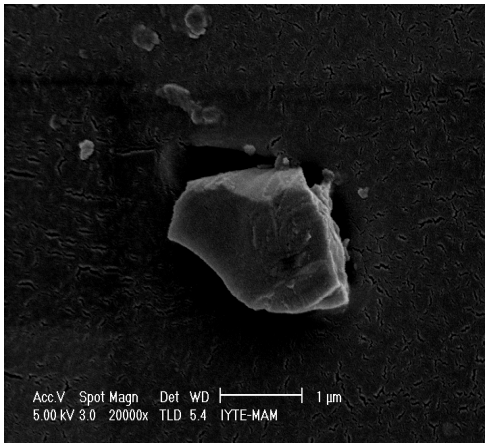

(*c*)

Figure 5.9. The microscopic pictures of optical thin films and the orientation of zeolites used in polarization measurements.

Second measurements performed on dielectric optical films of specific two groups used in LCD technology. The measurements results and polarization states given in Table 5.3 for the input state and in Table 5.4 for the output measurements.

Table 5.3.Reference (Input) Polarization State (3^0/103^0)		
I_p	I_s	$p_0=(I_p-I_s)/(I_p+I_s)$
4400	380	0.841

Table 5.4. Forward scattering measurements ($\theta=0^0$) for different dielectric films [λ=633nm]

Optical Film	I_p	I_s	$I_{\max}$	$I_{\min}$	$p_0=(I_p-I_s)/(I_p+I_s)$	$p_{out}=\frac{I_{\max}-I_{\min}}{I_{\max}+I_{\min}}$	Polarization State
S1	30	1	30	1	0.9355	0.9355	P_0
S2	34	1	40	1	0.9429	0.9512	22
S3	33	1	36	1	0.9412	0.9459	21
S4	0	0	0	0	x	x	x
C1	30	0	30	0	1.0000	1.0000	P_0
C2	0	0	0	0	x	x	x
C3	18	3	18	3	0.7143	0.7143	P_0
C4	0	0	0	0	x	x	x

Filters *S2* and *S3* significantly changed the polarization state of the incident light at the output. *S1*, *C1* and *C3* remained without change in polarization state, however *C1* filter acting as perfect linear polarizer, obtained an enhancement in degree of linear polarization. Since filters *S4*, *C2* and *C4* are excellent diffusers, all forward scattering measurements ($\theta = 0$) recorded as zero.

CHAPTER 6

RESULTS AND CONCLUSION

The main aim of this thesis work is to find out a way of exploiting the polarization discrimination properties of scattered light by nonspherical dielectric particles in order to improve the brightness in LCD backlight systems. For those purposes suitable scatterers such as prolate and oblate spheroids are analyzed and percentage improvement, the results are presented below. A typical LCD backlight system is depicted in Fig. 6.1.

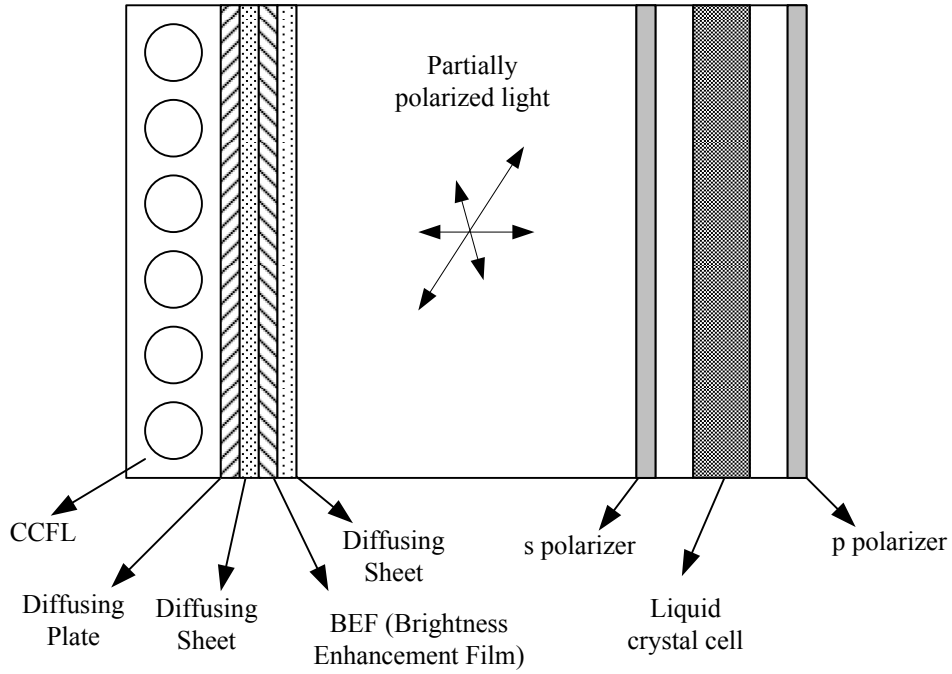

Figure 6.1. Shematic picture of typical direct backlight LCD system

The light produced by CCF Lamps is incoherent, unpolarized and occupying the range of the visible spectrum. In a typical LCD backlight system, the light passes through the optical films, which are cascaded in the order of diffusing plate, diffusing sheet, BEF and top diffusing sheet, the light is still unpolarized and incoherent with a slight change in the spectral distribution.

In general, dielectric homogeneous spherical particles are used in the diffusing

plate and the diffusing sheets, which do not have a morphological asymmetry and do not show any polarization differentiation. However, the films containing nonspherical scatterers can exhibit polarization discrimination in a favored direction, and the light is characterized as partial polarized in contrast to unpolarized in classical case.

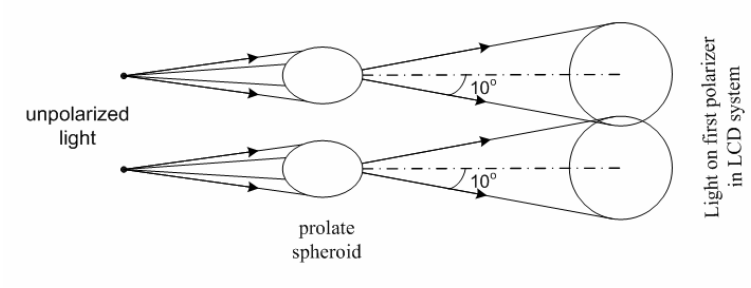

Figure 6.2. Scatterer geometry used in LCD system

In the LCD backlight system the light needs to be mostly scattered in the forward direction in order to increase efficiency, and the brightness. In general the polarizer is placed in the system at very close to both the films and the cell unit. Therefore, a small angle can be considered as the angle of contribution at the pixel spacing and the scatterer position, shown in Fig.6.2. As shown in the Fig.6.2 and Fig.6.3 most of the light on the polarizer is coming from the nearest (direct) scatterer. However, the contribution from the neighbor scatters can simply be added if they are polarized in the same direction since the light is still incoherent.

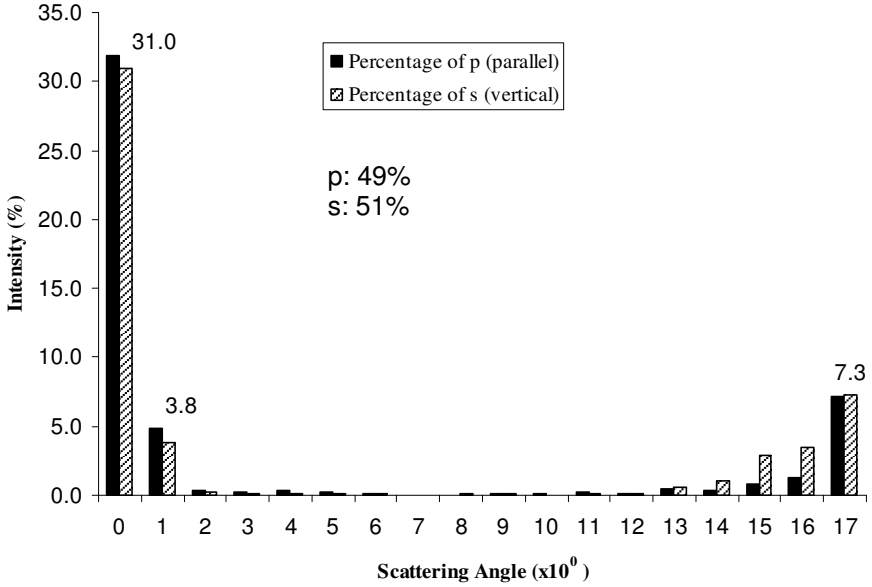

Figure 6.3. Intensity distribution percentages of *s* and *p*- polarized components for a sphere a=b=c=4μm (λ=632.8nm)

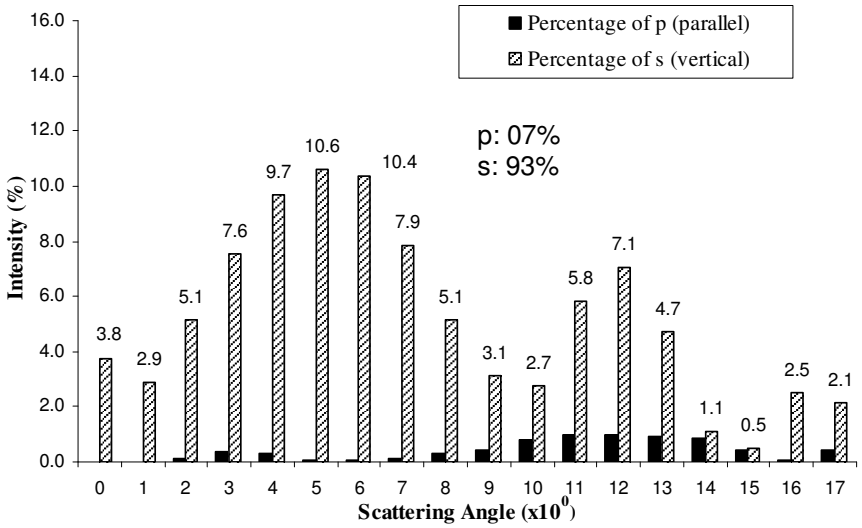

Figure 6.4. Intensity distribution percentages of *s* and *p*- polarized components for a prolate spheroid c/a=3.75 (λ=632.8nm)

As a reference the spherical scatterer is simulated for the normal incident, the scattering graphic is shown in the Figure 6.3. The most of the power is within the angle of a few degree and the polarizations are equal in p (parallel) and s (vertical) states.

When the scatterer is prolate spheroid in shape and have large aspect ratio (c/a), the simulation results at the normal incident are presented in the Figure 6.4, a significant polarization discrimination even at small scattering angles is shown. The polarization is dominantly in the favor of s-state (93 %) and the power spreads all over for forward scattering angles. On the other hand the simulation results for the oblate spheroid shows less significant effects on polarization discrimination compared to the results of the prolate one. It is still slightly more polarization discriminating compared to the results for the spherical ones. The most significant polarization discrimination is obtained for spheroid particles with $c/a = 3.75$. The results indicate that the spherical and the small prolate particles produce no significant polarization discrimination effects at small scattering angles. Therefore, those particles can not be used for polarization enhancement purposes.

As a whole display system a favorable polarization direction of the backlight unit can be matched with the orientation of the polarizer such that the maximum power will be transmitted. In the case of the spherical particles only 50 % will be transmitted at most (on the graphic 40 %) , on the other hand; the spheroid particles having the aspect ratio 3.75 will be transmitting 63 % for over all forward scattering direction. Therefore, 13 % improvement can easily be achieved by replacing the films having spherical

scatters with the films having spheroid scatters. At this point, uniformity in the brightness and spectral distribution should also be considered. In the case of spheroids, the brightness distribution over the scattering angles suggests that it is easier to achieve uniformity due to higher scattering angles.

Polarization measurements are performed on optical films of two groups used in LCD backlights and on model films with and without nonspherical zeolite particles prepared in the laboratory. Two groups of filters exhibit no polarization discrimination at all. Existence of zeolite particles in the film resulted in significant polarization differentiation at forward scattering angles. This effect is stronger at one polarization direction with respect to the orthogonal one. However, SEM pictures of these films revealed that zeolite particles are not uniformly distributed and not as homogeneous particles. Therefore, it is not possible to obtain a uniform brightness with these films.

The results obtained for prolate spheroid dielectric particles with sizes 4-5 times of the wavelength show that the brightness improvement in LCD backlight units can be as high as 13 % or equivalently reducing one of the CCFL number.

REFERENCES

Ayrancı, I., Vaillon, R., Selçuk N., 2007. "Performance of discrete dipole approximation for prediction of amplitude and phase of electromagnetic scattering by particles", *Journal of Quantitative Spectroscopy &Radiative Transfer* Vol. 103, pp. 83–101

Born, M. and Wolf, E., 1986. *Principles of Optics* 6th edition (Cambridge University Press, United kingdom), pp.544-554

Born, M. and Wolf, E., 1999. *Principles of Optics* 7th (expanded) edition (Cambridge University Press , United kingdom), p.630.

Boyd, W.R., 2003. *Nonlinear Optics* 2nd. edition, pp.371-375.

Duparre´A., 2005. "Scattering From Surfaces and thin films-*Encyclopedia of Modern Optics*", p:314

Eremin, Y.A. 2005. *Scattering Theory-Encyclopedia of Modern Optics*, pp.326-330.

Firdous,S., Ikram,M., 2004. "Charactrization of turbid medium through diffusely backscattered polarized light with matrix calculus-I", *IEEE proceeding INCC 2004*, 115-23

Fujiwara H., 2007. "Spectroscopic Ellipsometry: Principles and Applications" (John Wiley & Sons, Ltd), pp.1-2

Germer, T.A. and Sung, L., 1999. "Polarized Light Scattering Measurements Of Roughness, Subsurface Defects, Particles, And Dielectric Layers On Silicon Wafers", *Proceedings of the Fourth Conference on Electromagnetic and Light Scattering by Nonspherical Particles. Theory and Applications*, held in Vigo, Spain, September 20-21, 1999.

Guenther, B.D., 2005. *Matrix Analysis-Encyclopedia of Modern Optics*, pp.205-210.

Hilfiker, J. N., Woollam J. A., 2005. "Ellipsometry" Encyclopedia of Modern Optics p:297-307.

Jellison, G.E., 2004. "Generalized ellipsometry for materials characterization", *Thin Solid Films,* vol. 450 pp.42–50.

Kalimanova, I., Ilieva N. and Georgieva, M., 2005. "Ellipsometry and Thin Films Parameters Measurement" *28th Int. Spring Seminar on Electronics Tech.*, pp.473-476.

Mishchenko, M.I., Travis, L.D., Lacis, A.A., 2002. “Scattering, Absorption, and Emission of Light by Small Particles”, third electronic release (Cambridge University Press, New york), pp. 147-152.

Nezhuvingal, A., Li, Y., Anumula, H. and Cameron, B.D., 2003, "Mueller matrix optical imaging with application to tissue diagnostics", *Proc. SPIE*, vol. 4961, pp. 24-33.

Saleh, B. E. A. and Teich, M. C., 1991 “Fundamentals of Photonics”, (Wiley, New York), pp.196- 205

Van de Hulst, H.C., 1981. “Light scattering by small particles” (Dover, New York,), pp.14-45, pp.128-130

WEB_1, 2007. Hyperphysics’s web site, 30/04/2007, http://hyperphysics.phy-tr.gsu.edu/hbase/phyopt/quarwv.html

WEB_2, 2007. Jack’s web site, 23/04/2007, http://www.kw.igs.net/~jackord/ee/e7.html

WEB_3, 2007. Jack’s web site, 23/04/2007, http://www.kw.igs.net/~jackord/j6.html

WEB_4, 2007. CSU’s web site, 20/03/2007, http://www.chm.colostate.edu/ Spectroscopic Ellipsometry.mht

WEB_5, 2007. Scatlab’s web site, 8/03/2007, http://www.scatlab.com

WEB_6, 2007. T-matrix’s web site, 10/03/2007, http://www.t-matrix.de

WEB_7, 2007. OGI’s web site, 11/04/2007, http://omlc.ogi.edu/classroom/ece532/class3/mie_math.html

Wolff, L.B., 1997. “Polarization Vision: A New Sensory Approach to Image Understanding,” *Image and Vision Computing*, vol. 15, pp.81-93.

Wriedt, T., 2002. “Using the T-Matrix Method for Light Scattering Computations by Non-axisymmetric Particles: Superellipsoids and Realistically Shaped Particles”, *Part. Part. Syst. Charact.* Vol.19, pp. 256- 268.

Wriedt, T., 1998. “A Review of Elastic Light Scattering Theories”, *Part. Part. Syst. Charact.* Vol.15, pp. 67- 74.

Yevgen, G., Yuriy S., Gorden V., 2006. “Polarization of near-forward-scattered light from particulate substrates illuminated at near-grazing angles” *Journal of Quantitative Spectroscopy &Radiative Transfer* 101 p. 522–526

APPENDIX A

BLOCK ELEMENTS OF MATRIX *X*

The block elements of matrix $\boldsymbol{X}$ given in Equation 4.11 for $\boldsymbol{X}=\boldsymbol{A}$, $\boldsymbol{X}=\boldsymbol{B}$ and $\boldsymbol{X}=\boldsymbol{A}_0$ are given as (A.1), (A.2), and (A.3) respectively. m is the refractive index given by $m=\sqrt{\varepsilon_i/\varepsilon_s}$.

$$\left.\begin{aligned}
\boldsymbol{A}_{\nu\mu}^{11} &= \int_S \left[\left(n\times\Psi_\mu^1\right).\Psi_\nu^3 + m\left(n\times\varphi_\mu^1\right).\varphi_\nu^3\right]dS,\\
\boldsymbol{A}_{\nu\mu}^{12} &= \int_S \left[\left(n\times\varphi_\mu^1\right).\Psi_\nu^3 + m\left(n\times\varphi_\mu^1\right).\varphi_\nu^3\right]dS,\\
\boldsymbol{A}_{\nu\mu}^{21} &= \int_S \left[\left(n\times\Psi_\mu^1\right).\varphi_\nu^3 + m\left(n\times\varphi_\mu^1\right).\Psi_\nu^3\right]dS,\\
\boldsymbol{A}_{\nu\mu}^{22} &= \int_S \left[\left(n\times\varphi_\mu^1\right).\varphi_\nu^3 + m\left(n\times\varphi_\mu^1\right).\Psi_\nu^3\right]dS,
\end{aligned}\right\} \tag{A.1}$$

$$\left.\begin{aligned}
\boldsymbol{B}_{\nu\mu}^{11} &= \frac{jk_s^2}{\pi}\int_S \left[\left(n\times\Psi_\mu^1\right).\boldsymbol{N}_{\bar{\nu}}^1 + m\left(n\times\varphi_\mu^1\right).\boldsymbol{M}_{\bar{\mu}}^1\right]dS,\\
\boldsymbol{B}_{\nu\mu}^{12} &= \frac{jk_s^2}{\pi}\int_S \left[\left(n\times\varphi_\mu^1\right).\boldsymbol{N}_{\bar{\nu}}^1 + m\left(n\times\Psi_\mu^1\right).\boldsymbol{M}_{\bar{\mu}}^1\right]dS,\\
\boldsymbol{B}_{\nu\mu}^{21} &= \frac{jk_s^2}{\pi}\int_S \left[\left(n\times\Psi_\mu^1\right).\boldsymbol{M}_{\bar{\nu}}^1 + m\left(n\times\varphi_\mu^1\right).\boldsymbol{N}_{\bar{\mu}}^1\right]dS,\\
\boldsymbol{B}_{\nu\mu}^{22} &= \frac{jk_s^2}{\pi}\int_S \left[\left(n\times\Psi_\mu^1\right).\boldsymbol{M}_{\bar{\nu}}^1 + m\left(n\times\Psi_\mu^1\right).\boldsymbol{N}_{\bar{\mu}}^1\right]dS,
\end{aligned}\right\} \tag{A.2}$$

$$\left.\begin{aligned}
\boldsymbol{A}_{0\nu\mu}^{11} &= \int_S \left[\left(n\times\boldsymbol{M}_\mu^1\right).\Psi_\nu^3 + m\left(n\times\boldsymbol{N}_\mu^1\right).\varphi_\nu^3\right]dS,\\
\boldsymbol{A}_{0\nu\mu}^{12} &= \int_S \left[\left(n\times\boldsymbol{N}_\mu^1\right).\Psi_\nu^3 + m\left(n\times\boldsymbol{M}_\mu^1\right).\varphi_\nu^3\right]dS,\\
\boldsymbol{A}_{0\nu\mu}^{21} &= \int_S \left[\left(n\times\boldsymbol{M}_\mu^1\right).\varphi_\nu^3 + m\left(n\times\boldsymbol{N}_\mu^1\right).\Psi_\nu^3\right]dS,\\
\boldsymbol{A}_{0\nu\mu}^{22} &= \int_S \left[\left(n\times\boldsymbol{N}_\mu^1\right).\varphi_\nu^3 + m\left(n\times\boldsymbol{M}_\mu^1\right).\Psi_\nu^3\right]dS,
\end{aligned}\right\} \tag{A.3}$$

APPENDIX B

ELLIPSOID

Ellipsoidal particles are characterized by the three semiaxes $a \geq b \geq c$. If two of these axes have identical length, the ellipsoid is called spheroid. Generally, the shape of an aspherical particle is defined by its aspect ratio, which is the diameter of the particle divided by its length. Thus, a particle with an aspect ratio larger than one is a oblate particle and a particle with an aspect ratio smaller than one is a prolate particle.

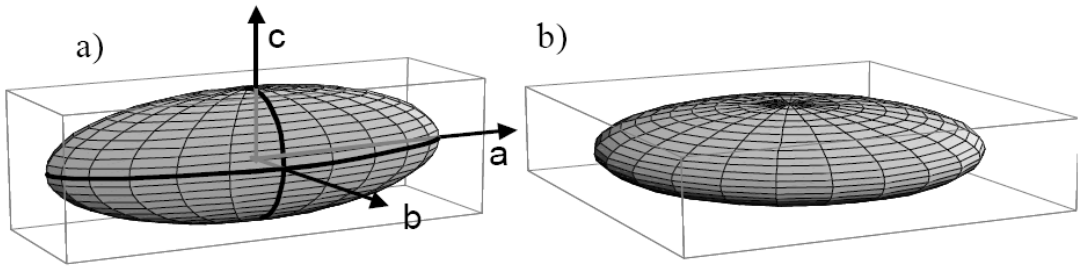

Figure B.1. a)prolate spheroid (a > b = c), b)oblate spheroid (a = b > c)